Journal of Quantitative Spectroscopy & Radiative Transfer 113 (2012) 1195–1219

Contents lists available at SciVerse ScienceDirect

Journal of Quantitative Spectroscopy & Radiative Transfer

journal homepage: www.elsevier.com/locate/jqsrt

Frequency and intensity analyses of the far infrared ν_5 band system of cyanogen (C_2N_2) and applications to Titan

A. Fayt [a], A. Jolly [b,*], Y. Benilan [b], L. Manceron [c,d], F. Kwabia-Tchana [b], J.-C. Guillemin [e]

[a] Laboratoire de Spectroscopie Moléculaire, Université Catholique de Louvain, Chemin du Cyclotron, 2 bte L7.01.07, B-1348 Louvain-La-Neuve, Belgium
[b] LISA—Laboratoire Interuniversitaire des Systèmes Atmosphériques, UMR 7583 du CNRS, Universités Paris 7 et 12, 61 Avenue du Général de Gaulle, 94010 Créteil Cedex, France
[c] Synchrotron SOLEIL, L'orme des Merisiers, Saint-Aubin-BP 48, 91192 Gif-sur-Yvette Cedex, France
[d] LADIR, CNRS-U. Paris 6, 4, place Jussieu 75252, France
[e] École Nationale Supérieure de Chimie de Rennes, Université de Bretagne, CNRS, UMR 6226, Avenue du Général Leclerc, CS 50837, 35708 Rennes Cedex 7, France

ARTICLE INFO

Available online 14 February 2012

Keywords:
Global analysis
Band intensities
Cyanogen
Hot bands
Titan
Far infrared
Linear molecules

ABSTRACT

The far infrared spectrum of cyanogen has been studied at high resolution to improve the rotational analysis of the ν_5 band system around 234 cm^{-1}. Present in the sample in natural abundances, both isotopologues $N^{13}CCN$ and $^{15}NCCN$ have also been studied. The weak ν_4–ν_5 difference band centered at 270 cm^{-1} has been studied for the first time. On the basis of a global rovibrational analysis limited to the ν_2, ν_4, and ν_5 modes, energy levels up to 2300 cm^{-1} have been considered to contribute to the overall spectrum intensity at room temperature leading to a new line list of 196,994 lines. The line intensity prediction has been used to correct previous line intensity measurements by taking into account line mixing. A new vibrational transition moment has been deduced and compared to new band intensity measurements obtained by low resolution studies which are also presented in this paper. The agreement between both approaches is very good and rules out the apparent disagreement between line intensity and band intensity measurements observed in the past. An intensity study of $^{15}NCCN$ is also proposed here thanks to the availability of a pure sample. Those results open the way to the search for isotopologues of cyanogen in Titan's atmosphere.

1. Introduction

Cyanogen was first identified in Titan's atmosphere in 1981 [1] by the infrared spectrometer IRIS on board the Voyager spacecraft. The detection has been later confirmed by the infrared instrument CIRS of the CASSINI mission [2]. The quality of the new observations has even allowed to detect cyanogen on Titan at equatorial and southern latitudes for the first time with abundances as low as 5×10^{-11} [3]. The abundance reaches a maximum of 3×10^{-9} in the north polar region, showing an important enrichment towards northern latitudes, in agreement with the behavior observed for other species. All the detections are done in the far infrared at 234 cm^{-1} through the only infrared active bending mode ν_5. It is also, by far, the strongest feature in the whole infrared domain and in most conditions the unique detection possibility. Together with the absence of any rotational spectra, this is probably the reason why cyanogen has so far not been detected in any other spatial environment.

At the time of the first detection of C_2N_2, the fundamental vibration frequencies were relatively well established, including the ν_5 infrared active mode which

* Corresponding author. Tel.: +33 145171540; fax: +33 145171564.
E-mail address: jolly@lisa.u-pec.fr (A. Jolly).

0022-4073/$ - see front matter © 2012 Elsevier Ltd. All rights reserved.
doi:10.1016/j.jqsrt.2012.02.003

was observed by Jones [4]. A rotational analysis of ν_5 was provided by Jolma [5] at medium resolution (0.02 cm^{-1}) and later at high resolution (0.0018 cm^{-1}) by Grecu et al. [6]. In that work, the assignments were limited to the ν_5 manifold up to $\upsilon_5=4$, although many hot bands involving the ν_4 and ν_2 infrared inactive modes and higher υ_5 values are expected to contribute to the spectrum. The stimulated Raman spectrum of the ν_2 stretching mode has been observed and analyzed by Bermejo et al. [7]. In 2003, the collaboration of the Giessen group with Maki has considerably improved the knowledge about the infrared spectrum of cyanogen for the doubly substituted species $N^{13}C^{13}CN$ and $^{15}NCC^{15}N$ [8], but the corresponding analysis for the normal species was not published up to very recently [9]. The opportunity to record the ν_5 band at the synchrotron radiation facility SOLEIL and the development of a global rovibrational analysis for NCCN were the occasion to improve the knowledge of the cyanogen energy levels up to about 2000 cm^{-1} (the ν_1 and ν_3 modes appear at higher energies and are outside the scope of this work).

Concerning the intensities, band intensity measurements at low resolution have been carried out for the ν_5 mode by Miyazawa [10] and Kim and King [11] with a good agreement, confirmed by the theoretical predictions of Botschwina and Sebald [12]. Nevertheless, line intensities measured by Grecu et al. [13] show a large disagreement with Kim and King when comparing the vibrational transition moments derived in both studies. This difference, corresponding to almost a factor of 2 in intensity, was one of the motivations for this new study on the ν_5 band of cyanogen. Another motivation was to extend the line list of C_2N_2 used to analyze the observations in order to improve the radiative transfer modeling and get the chance to detect and quantify isotopic species of cyanogen in Titan's atmosphere. Improvements in the knowledge of spectroscopic parameters have recently been successful, leading to the detection of ^{13}C and ^{15}N bearing molecules in Titan's atmosphere including $H^{13}CCCN$ [14], $H^{13}CCCCH$ [15], $H^{13}CN$, and $HC^{15}N$ [16]. While the $^{12}C/^{13}C$ isotopic ratio was measured in Titan for many molecules and found to be close to the terrestrial value [17], the $^{14}N/^{15}N$ isotopic ratio was only measured in the infrared for HCN [16] and in-situ by the Huygens probe for N_2 [18], showing strong enrichment in ^{15}N by a factor 4.9 and 1.8, respectively. After failing to detect $HCCC^{15}N$ [14], cyanogen is the only nitrile left to look for ^{15}N in Titan's atmosphere. Better spectroscopic parameters are also necessary, in the frame of Titan studies, for molecules like propane for which recent studies have led to significant improvements in the analysis of Titan's infrared spectra [19,20,21].

In this paper, we present both high and low resolution laboratory spectra of cyanogen. Experimental details are presented, followed by the assignment of the high resolution spectrum. The principle of the global rovibrational analysis is explained, followed by the model used for the main interactions. Resulting molecular and effective parameters are presented for the ν_5 band system, the ν_4–ν_5 band and for both $^{15}NCCN$ and $N^{13}CCN$ which are observed in natural abundance. We present a new determination of the vibrational transition moment of the ν_5 mode deduced from Grecu's line intensity measurement and the first determination of the intensity of the ν_4–ν_5 band. Results from low resolution experimental spectra are also presented and, in particular, a new determination of the integrated band intensity of ν_5 for the main isotopologue, as well as for $^{15}NCCN$. The comparison between band intensities and line intensity measurements is discussed and relevant formulas are given. Finally, new line lists are used to test the possible detection of $^{15}NCCN$ in Titan's atmosphere.

The conventional normal mode numbering for cyanogen is used throughout this paper. Modes 1 to 5 correspond to the symmetric CN σ_g^+ (ν_1) and CC σ_g^+ (ν_2) stretches, the antisymmetric CN stretch σ_u^+ (ν_3), and the *trans*$-\pi_g$ (ν_4) and *cis*$-\pi_u$ (ν_5) doubly degenerate bends. Labels n and t refer to stretching and bending vibrational modes, respectively, and s or i refer to any vibrational mode. The bends are further characterized by the usual vibrational angular momentum quantum numbers, ℓ_4 and ℓ_5, with $k=\ell_4+\ell_5$. In this paper, *state* refers to a vibrational state characterized by the $(\upsilon_1\upsilon_2\upsilon_3\upsilon_4\upsilon_5)$ set of vibrational quantum numbers. *Substate* indicates a ℓ_i-component of a state identified using $(\upsilon_1\upsilon_2\upsilon_3\upsilon_4\upsilon_5,\ell_4\ell_5)$. In some cases, the classical notations $\upsilon_i^{\ell_i}$ and $v_i^{\ell_i}$ can be used for the degenerate modes, for the quantum numbers and the states, respectively. *Level* refers to a specific J-value of a state or substate. The symmetry labels include e/f [22] and u/g properties. The same labels apply to $N^{13}CCN$ and $^{15}NCCN$ which are also considered in this investigation, except the missing u/g character. For the intensity calculations, m is classically defined as $J+1$, J, or $-J$ for $R(J)$, $Q(J)$, or $P(J)$ lines, respectively.

2. Experimental details

2.1. Synthesis and purification procedure

The sample of normal cyanogen was prepared in a flask containing AgCN (1.0 g, 7.5 mmol) that was adapted to a U-tube equipped with stopcocks in a vacuum line (0.1 mbar). The *U*-tube was immersed in a liquid nitrogen bath and the flask was heated with a Bunsen burner for about 2 min to form, via the cyanogen radical, the cyanogen molecule NCCN which was trapped in the *U*-tube. The stopcocks of the *U*-tube were then closed and the cyanogen (120 mg, 2.3 mmol) was finally obtained with a 62% yield.

The mono-labeled cyanogen ^{15}N has been synthesized in a two-step sequence using the approach of Wilmes and Winnewisser [23]. After dehydration of the oxamide with phosphorus pentaoxide and sea sand, the labeled cyanogen was trapped with huge amounts of carbon dioxide as shown in the following scheme:

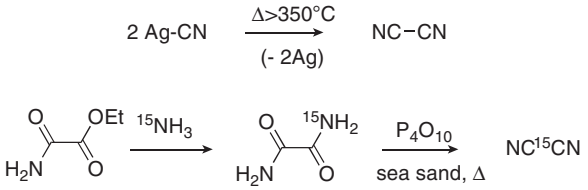

The solid sample was then kept at −90 °C and connected through a vacuum line to a 5 m path length White cell (2.2 L). The vapor phase was controlled by infrared spectra between 500 and 4500 cm^{-1} at 0.5 cm^{-1} resolution (Bruker Vertex 70). Observed traces of CO_2 disappeared after only a few evaporation sequences. Further purification was performed since $H^{15}NCO$ and $HC^{15}N$ were identified during the recording of the first far infrared spectra and by mass spectrometry as secondary mass appeared, respectively, at 44 and 28*m*/*e*. The sample was pumped while being kept at −50 °C which allowed to get rid of both impurities leaving a pure sample (>98%) of $^{15}NCCN$.

2.2. High resolution spectra

High resolution cyanogen spectra were recorded at the synchrotron radiation facility SOLEIL in France using the Fourier Transform spectrometer (Bruker IFS125HR) at the AILES beam line. It was equipped with a 6 μm mylar multilayer beam splitter and a liquid helium cooled Si bolometer detector. All spectra were obtained with a Globar source, an aperture diameter of 3.15 mm, and recorded at room temperature (296.5 K) using a multipass cell of 20 cm base length for a total optical path of 564.9 cm.

The high resolution spectrum was recorded between 115 and 320 cm^{-1} at 0.002 cm^{-1} resolution with a 0.2 mbar pure sample of cyanogen and averaged over a total recording time of 82 h. About 13,000 peak positions were determined between 180 and 300 cm^{-1} using the available Bruker software which also provides the absorbance of the line. The high density of lines can be seen in Fig. 1 as well as the good signal to noise ratio in the enlargement.

On the high frequency side of the ν_5 band centered at 234 cm^{-1}, we can see the weak ν_4–ν_5 parallel difference band with a band center at 270 cm^{-1} which is observed for the first time. The *R*-branch is clean, with a maximum at about 277 cm^{-1}, while the *P*-branch is buried under the ν_5 band.

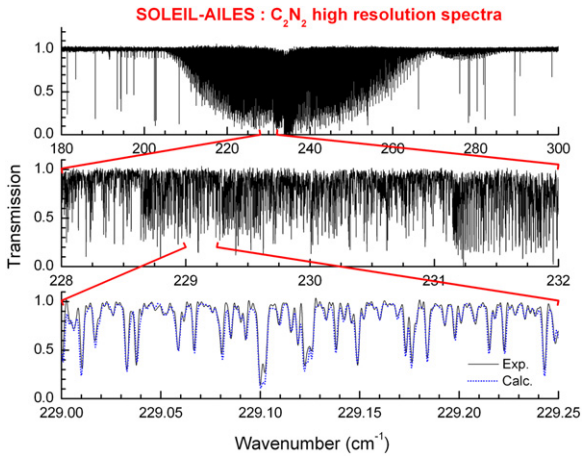

Fig. 1. High resolution (0.002 cm^{-1}) spectra of the ν_5 band system of cyanogen. A calculated spectrum is shown in the lower panel together with the experimental spectra.

Calibration was achieved with residual water lines observed in the spectra between 120 and 315 cm^{-1} using the HITRAN line list [24]. After a linear calibration, the deviation for about 30 water lines was found to be better than ±0.00005 cm^{-1} and on average ±0.00002 cm^{-1}. We observe a disagreement close to 0.001 cm^{-1} on the absolute line positions between this work and Grecu's older study on the normal isotope [6] but fully agree with Grecu's recent work on the monosubstituted isotopes [25] $^{15}NCCN$ and $N^{13}CCN$. All isotopes are measured in the same spectra in this work and submitted to the same calibration procedure. The agreement is very good with Grecu's recent study [25] and we therefore suspect a data manipulation problem in Grecu's older study on the normal isotope [6].

2.3. Low resolution spectra

Low resolution cyanogen spectra were also recorded at room temperature (296.5 K) with the same experimental apparatus. Band intensity measurements were recorded at various resolutions (0.05, 0.1, and 0.5 cm^{-1}) and different pressures of cyanogen between 0.05 and 0.5 mbar mixed with 800 mbar of nitrogen. The pressure broadening effect induced by nitrogen was found to be essential to avoid saturation effects. It was also found to be necessary to wait a minimum of two hours to obtain a homogenized sample characterized by a stable absorbance. Indeed, the recorded absorbance, after introducing the nitrogen to the sample, was monitored and progressed from a weaker value to a much stronger (about a factor 3) and very stable absorbance within two hours.

No impurities were observed in the sample of normal C_2N_2. Residual water lines are due to water present in the spectrometer but not in the sample. Band intensities were measured for 5 different pressures and two resolutions (0.1 and 0.5 cm^{-1}). Fig. 2 presents all five spectra in transmission at 0.5 cm^{-1} resolution. The spectrum at 0.110 mbar has been taken at the end of the measurements and shows a good reproducibility of the measurements when compared to the spectra taken at 0.109 mbar at the beginning. All spectra were integrated between 200

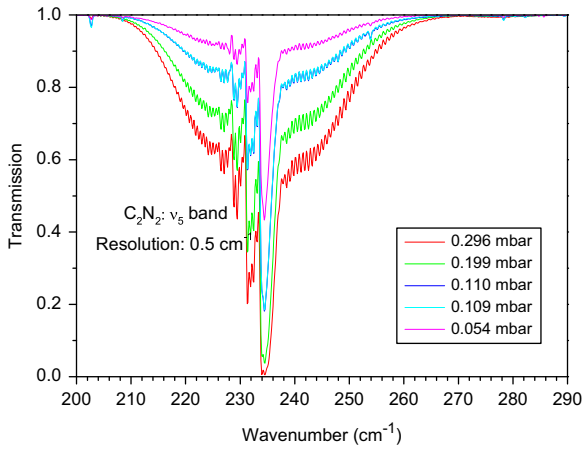

Fig. 2. Transmission spectra at various pressures showing the ν_5 band system of cyanogen at 0.5 cm^{-1} resolution.

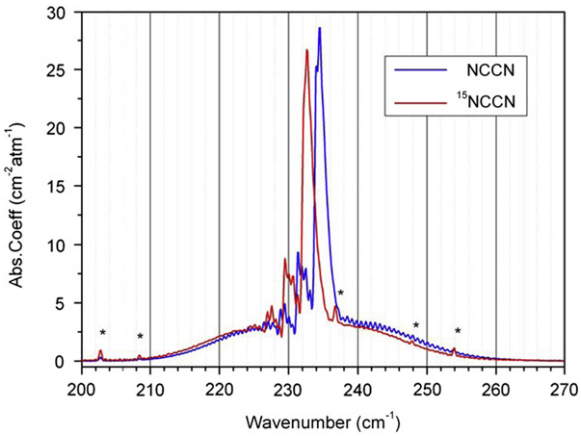

Fig. 3. Absorption coefficient of the ν_5 band system of NCCN and ^{15}NCCN (∗residual water lines).

and 290 cm^{-1} and resulting absorption coefficients were found to be consistent within a 5% margin.

We have also recorded low resolution spectra of ^{15}NCCN at three different pressures and three different resolutions. Impurities have been found in the sample of ^{15}NCCN to reach almost 10% in the first recorded spectra at 0.47 mbar. This percentage has been obtained by evaluating the quantity of HCN and HNCO through their infrared spectra. Two more spectra at 0.095 and 0.056 mbar have been recorded after purification of the sample showing residual impurities to reach only 2% of the total sample pressure. As the spectra at 0.47 mbar also showed sign of saturation on the Q branch, we have chosen to evaluate the band intensity for ^{15}NCCN from the spectra with lower pressures and a minimum of impurities. Spectra have been recorded at a resolution of 0.05, 0.1, and 0.5 cm^{-1} making a total of 6 spectra. Fig. 3 presents experimental absorption coefficients obtained from the average of all spectra mentioned above for both isotopologues. Compared to NCCN, the absorption of ^{15}NCCN is shifted down by 2 cm^{-1} and shows an intensity decrease of about 5%. It is the first band intensity measurement for this isotopologue.

3. Assignment of the high resolution spectra

The room temperature cyanogen spectrum between 200 and 300 cm^{-1} presents fundamental transitions and difference bands involving the ν_5 (234 cm^{-1}), ν_4 (503 cm^{-1}), and ν_2 (845 cm^{-1}) modes, up to energies of about 2000 cm^{-1}. The high number of substates results from the low energy of those modes and from the numerous ℓ-substates in the combinations of the ν_5 and ν_4 degenerate modes. Combined with the low spacing in R and P branches ($2B \approx 0.314$ cm^{-1}), this is responsible for the crowded aspect of the spectrum. The substates are perturbed by various ℓ-type resonances which destroy the usual regularity of energies according to $J(J+1)$. Furthermore, the identification of the substates and the prediction of their energy are difficult in most cases. For all those reasons, the classical band-by-band assignments and state-by-state analyses are creating problems in the case of cyanogen, except for a limited number of unperturbed states.

The assignment procedure is based on our global rovibrational analysis which will be described in detail in the next paragraph. This analysis takes into account explicitly all rotational and vibrational ℓ-type resonances and some anharmonic and Coriolis resonances, and fits simultaneously all polyads on the basis of a single set of molecular parameters. A first set of parameters has been obtained on the basis of a few data from Grecu's spectra [6]. Using those molecular parameters, we can calculate, for any J value, the eigenvalues and eigenvectors of any substate. Using them, another program automatically calculates the wavenumbers and the intensity of any line according to the vibrational selection rule and starting from polyads of increasing energy. For each predicted subband above some intensity threshold, we generate a diagram where the corresponding experimental lines are generally obvious if the prediction is not too bad. We check both the wavenumber regularity and the coherence of the intensities. We select some data, according to three possible procedures which are discussed later, and we associate an adequate uncertainty with each experimental wavenumber, according to the regularity and the dispersion of the series and the intensity of the line. The global analysis is improved step-by-step: new assignments, new fits giving improved or new parameters, more accurate predictions, new diagrams, and so on.

We present in Tables 1 and 2 a summary of the assigned subbands, 240 in the ν_5 band and 20 in the ν_4–ν_5 band, and we thank Maki for his help to find the important 00 020,00e − 00 011,1 − 1e band. An asterisk marks the assignments of the 18 subbands previously measured by Grecu et al. [6]. After the assignment, # corresponds to the number of lines in the subband selected for the global analysis in the J'-range defined by J_{min} and J_{max}. Sigma (cm^{-1}) is the estimated absolute uncertainty (one σ) for the unblended lines, 0.00005 cm^{-1} for a few very strong bands, 0.0001 or 0.0002 cm^{-1} for most bands, and from 0.0004 to 0.0008 cm^{-1} for the weakest bands. The next column lists the corresponding band centers (cm^{-1}), calculated on the basis of the vibrational energies E_ν (Section 4.5), and the last column gives the maximum calculated line intensity in the subband (in cm^{-2} atm^{-1} multiplied by 10^3). The strongest line in the whole spectrum is the cold band $Q(26)$ line with an intensity of 0.6143 cm^{-2} atm^{-1}, while the line detection threshold is around 0.0003 cm^{-2} atm^{-1}. Using the same intensity criterion, we were able to assign all bands above 0.0010 cm^{-2} atm^{-1}, most bands between 0.0010 and 0.0005 cm^{-2} atm^{-1}, and some bands between 0.0005 and 0.0002 cm^{-2} atm^{-1}.

We have also assigned, respectively, 14 and 10 subbands of the ν_5 band system of N^{13}CCN and ^{15}NCCN isotopologues. Those data partly overlap the 8 and 7 subbands of the ν_5 band system of the same isotopologues reported by Grecu et al. [25] in Tables 2 and 4 of their paper essentially devoted to the doubly substituted species and the substitution structure of cyanogen. We present in Table 3 a summary of all assigned subbands from both works, which have been introduced in our global analyses. Using Grecu's parameters in the usual

Table 1
Summary of the assigned subbands in the ν_5 band of NCCN.

Upper state							Lower state							#	J_{min}	J_{max}	Sigma	Band cent.	Intens.
0	0	0	0	1,	0	1eu	0	0	0	0	0,	0	0eg*	176	1	109	0.00005	233.7226	344.90
0	0	0	0	1,	0	1fu	0	0	0	0	0,	0	0eg*	22	2	107	0.00010	233.7226	614.28
0	0	0	0	2,	0	0eg	0	0	0	0	1,	0	1eu*	33	0	106	0.00005	231.1459	114.57
0	0	0	0	2,	0	0eg	0	0	0	0	1,	0	1fu*	11	2	79	0.00010	231.1459	176.56
0	0	0	0	2,	0	2eg	0	0	0	0	1,	0	1eu*	30	6	90	0.00005	234.1886	110.24
0	0	0	0	2,	0	2eg	0	0	0	0	1,	0	1fu	19	3	104	0.00010	234.1886	217.46
0	0	0	0	2,	0	2fg	0	0	0	0	1,	0	1fu*	36	4	103	0.00005	234.1886	119.84
0	0	0	0	2,	0	2fg	0	0	0	0	1,	0	1eu	22	4	99	0.00010	234.1886	197.10
0	0	0	0	3,	0	1eu	0	0	0	0	2,	0	0eg*	29	5	103	0.00010	231.6972	74.35
0	0	0	0	3,	0	1eu	0	0	0	0	2,	0	2eg*	20	2	73	0.00010	228.6545	14.58
0	0	0	0	3,	0	1eu	0	0	0	0	2,	0	2fg	11	5	69	0.00010	228.6545	28.33
0	0	0	0	3,	0	1fu	0	0	0	0	2,	0	2fg*	23	3	92	0.00010	228.6545	16.92
0	0	0	0	3,	0	1fu	0	0	0	0	2,	0	2eg	12	4	68	0.00010	228.6545	34.37
0	0	0	0	3,	0	1fu	0	0	0	0	2,	0	0eg*	18	2	87	0.00010	231.6972	120.53
0	0	0	0	3,	0	3eu	0	0	0	0	2,	0	2eg*	27	7	91	0.00010	234.6546	61.17
0	0	0	0	3,	0	3eu	0	0	0	0	2,	0	2fg	23	19	95	0.00010	234.6546	96.33
0	0	0	0	3,	0	3fu	0	0	0	0	2,	0	2fg*	27	4	94	0.00010	234.6546	61.12
0	0	0	0	3,	0	3fu	0	0	0	0	2,	0	2eg	15	8	83	0.00010	234.6546	96.58
0	0	0	1	1,	1	−1eu	0	0	0	1	0,	1	0eg	15	7	89	0.00010	232.2424	16.82
0	0	0	1	1,	1	−1eu	0	0	0	1	0,	1	0fg	10	1	55	0.00020	232.2424	22.84
0	0	0	1	1,	1	−1fu	0	0	0	1	0,	1	0fg	27	2	86	0.00010	233.5736	21.79
0	0	0	1	1,	1	−1fu	0	0	0	1	0,	1	0eg	7	2	38	0.00020	233.5736	18.75
0	0	0	1	1,	1	1eu	0	0	0	1	0,	1	0eg	17	9	71	0.00010	233.7077	14.09
0	0	0	1	1,	1	1eu	0	0	0	1	0,	1	0fg	9	5	57	0.00020	233.7077	31.32
0	0	0	1	1,	1	1fu	0	0	0	1	0,	1	0fg	14	6	56	0.00010	233.7076	11.73
0	0	0	1	1,	1	1fu	0	0	0	1	0,	1	0eg	10	4	62	0.00020	233.7076	39.41
0	0	0	0	4,	0	0eg	0	0	0	0	3,	0	1eu*	36	2	90	0.00010	229.2888	25.44
0	0	0	0	4,	0	0eg	0	0	0	0	3,	0	1fu*	14	4	78	0.00020	229.2888	35.04
0	0	0	0	4,	0	2eg	0	0	0	0	3,	0	1eu*	24	3	70	0.00010	232.2435	16.15
0	0	0	0	4,	0	2eg	0	0	0	0	3,	0	1fu	8	9	72	0.00020	232.2435	36.61
0	0	0	0	4,	0	2eg	0	0	0	0	3,	0	3eu	21	4	70	0.00010	226.2434	5.39
0	0	0	0	4,	0	2eg	0	0	0	0	3,	0	3fu	13	8	66	0.00020	226.2434	9.56
0	0	0	0	4,	0	2fg	0	0	0	0	3,	0	1fu*	24	9	85	0.00010	232.2435	19.06
0	0	0	0	4,	0	2fg	0	0	0	0	3,	0	1eu	14	2	74	0.00020	232.2435	29.98
0	0	0	0	4,	0	2fg	0	0	0	0	3,	0	3fu	22	5	73	0.00010	226.2434	5.39
0	0	0	0	4,	0	2fg	0	0	0	0	3,	0	3eu	13	9	62	0.00020	226.2434	9.53
0	0	0	0	4,	0	4eg	0	0	0	0	3,	0	3eu*	21	6	88	0.00010	235.1207	28.42
0	0	0	0	4,	0	4eg	0	0	0	0	3,	0	3fu	13	5	85	0.00020	235.1207	40.46
0	0	0	0	4,	0	4fg	0	0	0	0	3,	0	3fu*	23	7	87	0.00010	235.1207	28.44
0	0	0	0	4,	0	4fg	0	0	0	0	3,	0	3eu	16	5	84	0.00020	235.1207	40.41
0	0	0	1	2,	1	0eg	0	0	0	1	1,	1	−1eu	28	8	90	0.00010	231.4626	10.97
0	0	0	1	2,	1	0eg	0	0	0	1	1,	1	1eu	13	6	44	0.00020	229.9973	3.41
0	0	0	1	2,	1	0eg	0	0	0	1	1,	1	1fu	12	3	64	0.00020	229.9974	7.74
0	0	0	1	2,	1	0fg	0	0	0	1	1,	1	−1fu	19	21	81	0.00020	230.1315	3.07
0	0	0	1	2,	1	0fg	0	0	0	1	1,	1	−1eu	13	5	56	0.00020	231.4627	15.04
0	0	0	1	2,	1	0fg	0	0	0	1	1,	1	1fu	12	7	55	0.00040	229.9975	3.44
0	0	0	1	2,	1	0fg	0	0	0	1	1,	1	1eu	13	5	71	0.00020	229.9974	8.74
0	0	0	1	2,	−1	2eg	0	0	0	1	1,	1	−1eu	17	10	58	0.00020	234.3750	4.28
0	0	0	1	2,	−1	2eg	0	0	0	1	1,	1	−1fu	12	2	68	0.00020	233.0438	21.29
0	0	0	1	2,	−1	2eg	0	0	0	1	1,	1	1eu	10	27	62	0.00020	232.9098	1.04
0	0	0	1	2,	−1	2eg	0	0	0	1	1,	1	1fu	12	10	78	0.00020	232.9098	6.58
0	0	0	1	2,	−1	2fg	0	0	0	1	1,	1	−1fu	16	11	75	0.00010	233.0437	13.50
0	0	0	1	2,	−1	2fg	0	0	0	1	1,	1	−1eu	9	4	77	0.00020	234.3749	9.58
0	0	0	1	2,	−1	2fg	0	0	0	1	1,	1	1fu	6	43	59	0.00020	232.9097	0.90
0	0	0	1	2,	1	2eg	0	0	0	1	1,	1	1eu	19	10	74	0.00020	234.1793	10.86
0	0	0	1	2,	1	2eg	0	0	0	1	1,	1	1fu	13	10	80	0.00020	234.1794	16.84
0	0	0	1	2,	1	2fg	0	0	0	1	1,	1	1fu	25	3	73	0.00010	234.1793	10.59
0	0	0	1	2,	1	2fg	0	0	0	1	1,	1	1eu	11	12	77	0.00020	234.1793	17.55
0	0	0	1	2,	1	2fg	0	0	0	1	1,	1	−1fu	8	31	55	0.00040	234.3133	1.13
0	1	0	0	1,	0	1eu	0	1	0	0	0,	0	0eg	51	6	72	0.00010	237.9493	5.82
0	1	0	0	1,	0	1fu	0	1	0	0	0,	0	0eg	27	4	68	0.00010	237.9493	10.37
0	0	0	0	5,	0	1eu	0	0	0	0	4,	0	0eg	19	9	85	0.00010	229.9153	12.30
0	0	0	0	5,	0	1eu	0	0	0	0	4,	0	2eg	13	5	55	0.00040	226.9606	2.90
0	0	0	0	5,	0	1eu	0	0	0	0	4,	0	2fg	11	5	63	0.00020	226.9607	5.81
0	0	0	0	5,	0	1fu	0	0	0	0	4,	0	0eg	13	5	60	0.00020	229.9154	18.07

Table 1 (*continued*)

Upper state							Lower state							#	J_{min}	J_{max}	Sigma	Band cent.	Intens.
0	0	0	0	5,	0	1fu	0	0	0	0	4,	0	2eg	15	8	66	0.00020	226.9607	7.78
0	0	0	0	5,	0	1fu	0	0	0	0	4,	0	2fg	27	8	78	0.00010	226.9607	3.65
0	0	0	0	5,	0	3eu	0	0	0	0	4,	0	2eg	18	11	77	0.00010	232.7852	8.50
0	0	0	0	5,	0	3eu	0	0	0	0	4,	0	2fg	12	15	69	0.00020	232.7853	13.56
0	0	0	0	5,	0	3eu	0	0	0	0	4,	0	4eg	14	7	65	0.00020	223.9079	1.84
0	0	0	0	5,	0	3eu	0	0	0	0	4,	0	4fg	11	13	61	0.00020	223.9079	2.95
0	0	0	0	5,	0	3fu	0	0	0	0	4,	0	2fg	18	6	74	0.00020	232.7852	8.47
0	0	0	0	5,	0	3fu	0	0	0	0	4,	0	2eg	13	14	59	0.00020	232.7852	13.63
0	0	0	0	5,	0	3fu	0	0	0	0	4,	0	4fg	17	10	64	0.00020	223.9079	1.84
0	0	0	0	5,	0	3fu	0	0	0	0	4,	0	4eg	6	14	46	0.00020	223.9079	2.95
0	0	0	0	5,	0	5eu	0	0	0	0	4,	0	4eg	19	7	81	0.00010	235.5868	12.32
0	0	0	0	5,	0	5eu	0	0	0	0	4,	0	4fg	12	7	75	0.00020	235.5868	15.86
0	0	0	0	5,	0	5fu	0	0	0	0	4,	0	4fg	18	6	78	0.00010	235.5868	12.32
0	0	0	0	5,	0	5fu	0	0	0	0	4,	0	4eg	14	7	64	0.00020	235.5868	15.88
0	0	0	1	3,	1	−1eu	0	0	0	1	2,	1	0eg	18	5	81	0.00020	229.9274	5.16
0	0	0	1	3,	1	−1eu	0	0	0	1	2,	1	0fg	8	5	50	0.00020	229.9274	6.26
0	0	0	1	3,	1	−1fu	0	0	0	1	2,	1	0fg	6	26	42	0.00040	232.5063	1.14
0	0	0	1	3,	1	−1fu	0	0	0	1	2,	1	0eg	9	18	64	0.00040	232.5064	3.48
0	0	0	1	3,	1	−1fu	0	0	0	1	2,	−1	2fg	19	6	72	0.00020	229.5941	2.95
0	0	0	1	3,	1	−1fu	0	0	0	1	2,	−1	2eg	10	4	58	0.00020	229.5940	5.14
0	0	0	1	3,	1	1eu	0	0	0	1	2,	1	0eg	13	9	55	0.00020	231.7528	2.81
0	0	0	1	3,	1	1eu	0	0	0	1	2,	1	0fg	8	19	68	0.00020	231.7527	7.12
0	0	0	1	3,	1	1eu	0	0	0	1	2,	1	2eg	14	7	63	0.00040	227.5708	1.40
0	0	0	1	3,	1	1eu	0	0	0	1	2,	1	2fg	7	9	37	0.00020	227.5708	2.49
0	0	0	1	3,	1	1fu	0	0	0	1	2,	1	0fg	20	8	78	0.00020	231.7526	4.02
0	0	0	1	3,	1	1fu	0	0	0	1	2,	1	0eg	6	17	51	0.00040	231.7527	4.81
0	0	0	1	3,	1	1fu	0	0	0	1	2,	1	2fg	12	14	64	0.00040	227.5707	1.39
0	0	0	1	3,	1	1fu	0	0	0	1	2,	1	2eg	8	12	47	0.00040	227.5707	2.45
0	0	0	1	3,	−1	3eu	0	0	0	1	2,	−1	2eg	17	7	71	0.00020	233.7806	4.75
0	0	0	1	3,	−1	3eu	0	0	0	1	2,	−1	2fg	14	7	71	0.00020	233.7806	8.01
0	0	0	1	3,	−1	3fu	0	0	0	1	2,	−1	2fg	18	4	70	0.00020	233.7806	4.59
0	0	0	1	3,	−1	3fu	0	0	0	1	2,	−1	2eg	12	10	64	0.00040	233.7806	8.33
0	0	0	1	3,	1	3eu	0	0	0	1	2,	1	2eg	16	7	71	0.00020	234.6511	5.73
0	0	0	1	3,	1	3eu	0	0	0	1	2,	1	2fg	11	9	67	0.00020	234.6511	8.26
0	0	0	1	3,	1	3fu	0	0	0	1	2,	1	2fg	18	10	74	0.00020	234.6511	5.73
0	0	0	1	3,	1	3fu	0	0	0	1	2,	1	2eg	9	8	65	0.00040	234.6511	8.27
0	0	0	2	1,	2	−1eu	0	0	0	2	0,	2	0eg	25	7	61	0.00040	232.0388	1.28
0	0	0	2	1,	2	−1eu	0	0	0	2	0,	2	0fg	9	9	38	0.00040	232.0388	2.07
0	0	0	2	1,	2	−1fu	0	0	0	2	0,	2	0fg	18	8	56	0.00020	232.0388	1.28
0	0	0	2	1,	2	−1fu	0	0	0	2	0,	2	0eg	3	16	34	0.00040	232.0388	2.07
0	0	0	2	1,	2	1eu	0	0	0	2	0,	2	0eg	11	15	51	0.00020	233.6924	1.39
0	0	0	2	1,	2	1eu	0	0	0	2	0,	2	0fg	5	21	49	0.00040	233.6924	2.52
0	0	0	2	1,	2	1fu	0	0	0	2	0,	2	0fg	13	14	48	0.00020	233.6924	1.39
0	0	0	2	1,	2	1fu	0	0	0	2	0,	2	0eg	7	10	54	0.00040	233.6924	2.52
0	0	0	2	1,	0	1eu	0	0	0	2	0,	0	0eg	33	3	67	0.00040	233.1827	2.39
0	0	0	2	1,	0	1fu	0	0	0	2	0,	0	0eg	9	12	47	0.00040	233.1827	4.26
0	1	0	0	2,	0	0eg	0	1	0	0	1,	0	1eu	18	6	68	0.00040	235.0917	1.88
0	1	0	0	2,	0	0eg	0	1	0	0	1,	0	1fu	6	7	52	0.00040	235.0917	2.92
0	1	0	0	2,	0	2eg	0	1	0	0	1,	0	1eu	17	9	58	0.00040	238.2922	1.83
0	1	0	0	2,	0	2eg	0	1	0	0	1,	0	1fu	13	6	70	0.00040	238.2922	3.57
0	1	0	0	2,	0	2fg	0	1	0	0	1,	0	1fu	17	9	63	0.00040	238.2922	1.98
0	1	0	0	2,	0	2fg	0	1	0	0	1,	0	1eu	13	5	65	0.00020	238.2922	3.25
0	0	0	0	6,	0	0eg	0	0	0	0	5,	0	1eu	19	8	80	0.00020	227.6691	4.31
0	0	0	0	6,	0	0eg	0	0	0	0	5,	0	1fu	10	8	58	0.00020	227.6690	5.31
0	0	0	0	6,	0	2eg	0	0	0	0	5,	0	1eu	10	9	46	0.00020	230.5349	2.16
0	0	0	0	6,	0	2eg	0	0	0	0	5,	0	1fu	11	8	56	0.00020	230.5348	5.57
0	0	0	0	6,	0	2eg	0	0	0	0	5,	0	3eu	15	6	56	0.00020	224.7103	1.13
0	0	0	0	6,	0	2eg	0	0	0	0	5,	0	3fu	10	6	51	0.00020	224.7104	2.04
0	0	0	0	6,	0	2fg	0	0	0	0	5,	0	1fu	16	7	69	0.00020	230.5348	2.76
0	0	0	0	6,	0	2fg	0	0	0	0	5,	0	1eu	6	12	40	0.00020	230.5348	4.13
0	0	0	0	6,	0	2fg	0	0	0	0	5,	0	3fu	12	13	53	0.00020	224.7103	1.13
0	0	0	0	6,	0	2fg	0	0	0	0	5,	0	3eu	8	9	53	0.00020	224.7102	2.03
0	0	0	0	6,	0	4eg	0	0	0	0	5,	0	3eu	17	6	64	0.00020	233.3229	3.75
0	0	0	0	6,	0	4eg	0	0	0	0	5,	0	3fu	9	8	59	0.00040	233.3230	5.38
0	0	0	0	6,	0	4eg	0	0	0	0	5,	0	5eu	10	10	44	0.00020	221.6440	0.63
0	0	0	0	6,	0	4eg	0	0	0	0	5,	0	5fu	7	8	36	0.00040	221.6440	0.91
0	0	0	0	6,	0	4fg	0	0	0	0	5,	0	3fu	20	5	67	0.00020	233.3229	3.76
0	0	0	0	6,	0	4fg	0	0	0	0	5,	0	3eu	7	11	57	0.00020	233.3229	5.37

Table 1 (*continued*)

Upper state							Lower state							#	J_{min}	J_{max}	Sigma	Band cent.	Intens.
0	0	0	0	6,	0	4fg	0	0	0	0	5,	0	5fu	11	11	45	0.00020	221.6440	0.63
0	0	0	0	6,	0	4fg	0	0	0	0	5,	0	5eu	4	17	36	0.00040	221.6440	0.91
0	0	0	0	6,	0	6eg	0	0	0	0	5,	0	5eu	17	6	70	0.00020	236.0530	5.11
0	0	0	0	6,	0	6eg	0	0	0	0	5,	0	5fu	13	14	64	0.00020	236.0530	5.96
0	0	0	0	6,	0	6fg	0	0	0	0	5,	0	5fu	17	7	73	0.00020	236.0530	5.11
0	0	0	0	6,	0	6fg	0	0	0	0	5,	0	5eu	10	11	64	0.00020	236.0530	5.95
0	0	0	1	4,	1	0eg	0	0	0	1	3,	1	−1eu	11	6	54	0.00020	229.7520	2.48
0	0	0	1	4,	1	0eg	0	0	0	1	3,	1	1eu	8	8	38	0.00040	227.9267	0.67
0	0	0	1	4,	1	0eg	0	0	0	1	3,	1	1fu	6	11	36	0.00040	227.9268	1.28
0	0	0	1	4,	1	0fg	0	0	0	1	3,	1	1fu	16	9	57	0.00040	227.9268	1.00
0	0	0	1	4,	1	0fg	0	0	0	1	3,	1	1eu	6	5	45	0.00040	227.9267	1.96
0	0	0	1	4,	1	0fg	0	0	0	1	3,	1	−1eu	11	3	49	0.00040	229.7520	3.22
0	0	0	1	4,	−1	2eg	0	0	0	1	3,	1	1eu	6	28	56	0.00060	231.7134	0.58
0	0	0	1	4,	−1	2eg	0	0	0	1	3,	1	−1fu	4	2	30	0.00020	230.9597	4.21
0	0	0	1	4,	−1	2eg	0	0	0	1	3,	−1	3eu	4	34	42	0.00040	226.7731	0.47
0	0	0	1	4,	−1	2eg	0	0	0	1	3,	−1	3fu	4	18	36	0.00040	226.7732	0.92
0	0	0	1	4,	−1	2fg	0	0	0	1	3,	1	−1fu	17	13	63	0.00040	230.9598	2.33
0	0	0	1	4,	−1	2fg	0	0	0	1	3,	−1	3fu	4	26	39	0.00060	226.7732	0.43
0	0	0	1	4,	1	2eg	0	0	0	1	3,	1	1eu	17	4	50	0.00040	232.2667	1.67
0	0	0	1	4,	1	2eg	0	0	0	1	3,	1	1fu	4	11	30	0.00060	232.2668	2.80
0	0	0	1	4,	1	2fg	0	0	0	1	3,	1	1fu	12	5	47	0.00040	232.2667	1.67
0	0	0	1	4,	1	2fg	0	0	0	1	3,	1	1eu	6	27	53	0.00040	232.2666	2.83
0	0	0	1	4,	1	2fg	0	0	0	1	3,	1	3fu	7	13	28	0.00060	225.1863	0.49
0	0	0	1	4,	1	2fg	0	0	0	1	3,	1	3eu	5	13	51	0.00040	225.1863	0.78
0	0	0	1	4,	−1	4eg	0	0	0	1	3,	−1	3eu	14	8	58	0.00020	234.2884	2.25
0	0	0	1	4,	−1	4fg	0	0	0	1	3,	−1	3fu	14	12	61	0.00020	234.2884	2.25
0	0	0	1	4,	−1	4fg	0	0	0	1	3,	−1	3eu	9	15	58	0.00040	234.2884	3.52
0	0	0	1	4,	1	4eg	0	0	0	1	3,	1	3eu	16	10	64	0.00020	235.1227	2.66
0	0	0	1	4,	1	4eg	0	0	0	1	3,	1	3fu	9	19	62	0.00040	235.1227	3.47
0	0	0	1	4,	1	4fg	0	0	0	1	3,	1	3fu	13	8	55	0.00020	235.1227	2.66
0	0	0	1	4,	1	4fg	0	0	0	1	3,	1	3eu	9	15	61	0.00020	235.1227	3.46
0	0	0	2	2,	2	0eg	0	0	0	2	1,	2	−1eu	4	24	34	0.00040	231.0759	0.65
0	0	0	2	2,	2	0eg	0	0	0	2	1,	2	1eu	5	12	24	0.00060	229.4222	0.39
0	0	0	2	2,	2	0eg	0	0	0	2	1,	2	1fu	5	10	32	0.00060	229.4222	0.71
0	0	0	2	2,	2	0fg	0	0	0	2	1,	2	−1fu	11	13	51	0.00040	231.0759	0.59
0	0	0	2	2,	2	−2eg	0	0	0	2	1,	2	−1eu	9	14	40	0.00040	232.3692	0.65
0	0	0	2	2,	2	−2eg	0	0	0	2	1,	2	−1fu	5	12	44	0.00040	232.3692	1.65
0	0	0	2	2,	2	−2fg	0	0	0	2	1,	2	−1fu	11	7	45	0.00040	232.6152	0.68
0	0	0	2	2,	2	−2fg	0	0	0	2	1,	2	−1eu	5	13	41	0.00060	232.6152	1.60
0	0	0	2	2,	2	2eg	0	0	0	2	1,	2	1eu	15	12	56	0.00040	234.1696	1.02
0	0	0	2	2,	2	2eg	0	0	0	2	1,	2	1fu	5	28	46	0.00040	234.1696	1.51
0	0	0	2	2,	2	2fg	0	0	0	2	1,	2	1fu	9	9	49	0.00040	234.1696	1.01
0	0	0	2	2,	2	2fg	0	0	0	2	1,	2	1eu	5	19	46	0.00060	234.1696	1.51
0	0	0	2	2,	0	0eg	0	0	0	2	1,	0	1eu	15	9	60	0.00040	230.7213	0.79
0	0	0	2	2,	0	0eg	0	0	0	2	1,	0	1fu	11	6	44	0.00040	230.7213	1.23
0	0	0	2	2,	0	2eg	0	0	0	2	1,	0	1eu	11	12	54	0.00040	233.6484	0.77
0	0	0	2	2,	0	2eg	0	0	0	2	1,	0	1fu	12	10	62	0.00040	233.6484	1.51
0	0	0	2	2,	0	2fg	0	0	0	2	1,	0	1fu	13	11	46	0.00040	233.6484	0.83
0	0	0	2	2,	0	2fg	0	0	0	2	1,	0	1eu	3	8	19	0.00040	233.6484	1.37
0	1	0	0	3,	0	1eu	0	1	0	0	2,	0	0eg	15	15	59	0.00040	235.5177	1.20
0	1	0	0	3,	0	1fu	0	1	0	0	2,	0	0eg	7	6	54	0.00040	235.5177	1.95
0	1	0	0	3,	0	3eu	0	1	0	0	2,	0	2eg	8	21	49	0.00040	238.6370	1.00
0	1	0	0	3,	0	3eu	0	1	0	0	2,	0	2fg	10	7	49	0.00040	238.6370	1.55
0	1	0	0	3,	0	3fu	0	1	0	0	2,	0	2fg	14	12	50	0.00040	238.6371	1.00
0	1	0	0	3,	0	3fu	0	1	0	0	2,	0	2eg	8	16	46	0.00040	238.6370	1.56
0	0	0	0	7,	0	1eu	0	0	0	0	6,	0	0eg	16	9	67	0.00020	228.3714	1.84
0	0	0	0	7,	0	1eu	0	0	0	0	6,	0	2fg	9	15	51	0.00020	225.5057	0.91
0	0	0	0	7,	0	1fu	0	0	0	0	6,	0	0eg	11	4	50	0.00020	228.3714	2.45
0	0	0	0	7,	0	1fu	0	0	0	0	6,	0	2fg	11	8	58	0.00040	225.5057	0.62
0	0	0	0	7,	0	1fu	0	0	0	0	6,	0	2eg	10	12	50	0.00040	225.5056	1.34
0	0	0	0	7,	0	3eu	0	0	0	0	6,	0	2eg	10	19	51	0.00020	231.1489	1.13
0	0	0	0	7,	0	3eu	0	0	0	0	6,	0	2fg	9	13	47	0.00020	231.1489	1.82
0	0	0	0	7,	0	3eu	0	0	0	0	6,	0	4fg	6	9	47	0.00060	222.5363	0.63
0	0	0	0	7,	0	3fu	0	0	0	0	6,	0	2fg	14	16	54	0.00040	231.1489	1.12
0	0	0	0	7,	0	3fu	0	0	0	0	6,	0	2eg	4	16	46	0.00040	231.1489	1.84
0	0	0	0	7,	0	3fu	0	0	0	0	6,	0	4eg	5	14	46	0.00060	222.5362	0.63
0	0	0	0	7,	0	5eu	0	0	0	0	6,	0	4eg	11	17	49	0.00020	233.8568	1.58

Table 1 (*continued*)

Upper state							Lower state							#	J_{min}	J_{max}	Sigma	Band cent.	Intens.
0	0	0	0	7,	0	5eu	0	0	0	0	6,	0	4fg	7	19	45	0.00040	233.8569	2.04
0	0	0	0	7,	0	5fu	0	0	0	0	6,	0	4fg	15	14	52	0.00020	233.8569	1.58
0	0	0	0	7,	0	5fu	0	0	0	0	6,	0	4eg	5	23	48	0.00040	233.8568	2.04
0	0	0	0	7,	0	7eu	0	0	0	0	6,	0	6eg	15	7	53	0.00020	236.5194	2.05
0	0	0	0	7,	0	7eu	0	0	0	0	6,	0	6fg	5	15	46	0.00040	236.5194	2.16
0	0	0	0	7,	0	7fu	0	0	0	0	6,	0	6fg	19	8	64	0.00020	236.5194	2.05
0	0	0	0	7,	0	7fu	0	0	0	0	6,	0	6eg	8	14	46	0.00040	236.5194	2.16
0	0	0	1	5,	1	−1eu	0	0	0	1	4,	1	0eg	13	15	55	0.00040	228.0388	0.98
0	0	0	1	5,	1	−1eu	0	0	0	1	4,	1	0fg	6	18	32	0.00040	228.0388	1.10
0	0	0	1	5,	1	−1fu	0	0	0	1	4,	−1	2fg	6	16	32	0.00040	228.0108	0.70
0	0	0	1	5,	1	−1fu	0	0	0	1	4,	−1	2eg	8	10	38	0.00040	228.0108	1.07
0	0	0	1	5,	1	1eu	0	0	0	1	4,	1	0fg	9	11	45	0.00040	230.0798	1.21
0	0	0	1	5,	1	1fu	0	0	0	1	4,	1	0fg	8	16	40	0.00040	230.0798	0.62
0	0	0	1	5,	1	1fu	0	0	0	1	4,	1	0eg	8	8	30	0.00040	230.0798	0.80
0	0	0	1	5,	−1	3eu	0	0	0	1	4,	−1	2eg	6	11	41	0.00040	231.8094	0.67
0	0	0	1	5,	−1	3eu	0	0	0	1	4,	−1	2fg	4	9	23	0.00040	231.8094	1.07
0	0	0	1	5,	−1	3fu	0	0	0	1	4,	−1	2fg	6	20	30	0.00040	231.8094	0.60
0	0	0	1	5,	−1	3fu	0	0	0	1	4,	−1	2eg	4	20	32	0.00040	231.8095	1.19
0	0	0	1	5,	1	3eu	0	0	0	1	4,	1	2eg	6	23	41	0.00040	232.8030	0.81
0	0	0	1	5,	1	3eu	0	0	0	1	4,	1	2fg	5	19	37	0.00040	232.8031	1.18
0	0	0	1	5,	1	3fu	0	0	0	1	4,	1	2fg	5	30	40	0.00040	232.8030	0.81
0	0	0	1	5,	1	3fu	0	0	0	1	4,	1	2eg	3	22	28	0.00040	232.8029	1.17
0	0	0	1	5,	−1	5eu	0	0	0	1	4,	−1	4eg	5	15	29	0.00040	234.7693	0.99
0	0	0	1	5,	−1	5eu	0	0	0	1	4,	−1	4fg	6	25	45	0.00040	234.7693	1.40
0	0	0	1	5,	−1	5fu	0	0	0	1	4,	−1	4fg	3	21	30	0.00040	234.7693	0.99
0	0	0	1	5,	1	5eu	0	0	0	1	4,	1	4eg	10	9	51	0.00040	235.5942	1.15
0	0	0	1	5,	1	5eu	0	0	0	1	4,	1	4fg	6	19	47	0.00040	235.5942	1.36
0	0	0	1	5,	1	5fu	0	0	0	1	4,	1	4fg	14	8	52	0.00040	235.5941	1.15
0	0	0	0	8,	0	0eg	0	0	0	0	7,	0	1eu	22	8	58	0.00040	226.2990	0.65
0	0	0	0	8,	0	0eg	0	0	0	0	7,	0	1fu	3	24	42	0.00060	226.2990	0.73
0	0	0	0	8,	0	2eg	0	0	0	0	7,	0	1fu	15	4	62	0.00060	229.0707	0.80
0	0	0	0	8,	0	2fg	0	0	0	0	7,	0	1fu	12	15	53	0.00080	229.0706	0.38
0	0	0	0	8,	0	4eg	0	0	0	0	7,	0	3eu	5	20	42	0.00060	231.7596	0.48
0	0	0	0	8,	0	4eg	0	0	0	0	7,	0	3fu	6	16	42	0.00040	231.7596	0.70
0	0	0	0	8,	0	4fg	0	0	0	0	7,	0	3fu	4	19	29	0.00080	231.7596	0.48
0	0	0	0	8,	0	6eg	0	0	0	0	7,	0	5eu	14	8	44	0.00040	234.3876	0.64
0	0	0	0	8,	0	6fg	0	0	0	0	7,	0	5fu	7	16	47	0.00060	234.3876	0.64
0	0	0	0	8,	0	8eg	0	0	0	0	7,	0	7eu	10	12	37	0.00060	236.9862	0.81
0	0	0	0	8,	0	8eg	0	0	0	0	7,	0	7fu	5	21	33	0.00040	236.9862	0.77
0	0	0	0	8,	0	8fg	0	0	0	0	7,	0	7fu	9	12	37	0.00060	236.9861	0.81
0	0	0	0	8,	0	8fg	0	0	0	0	7,	0	7eu	5	17	33	0.00040	236.9861	0.77
0	0	0	1	6,	1	0eg	0	0	0	1	5,	1	−1eu	8	20	44	0.00060	228.1924	0.42
0	0	0	1	6,	−1	6eg	0	0	0	1	5,	−1	5eu	5	18	38	0.00060	235.2433	0.41
0	0	0	1	6,	1	6eg	0	0	0	1	5,	1	5eu	8	14	44	0.00060	236.0656	0.48
0	0	0	1	6,	1	6eg	0	0	0	1	5,	1	5fu	4	24	42	0.00040	236.0656	0.51
0	0	0	0	9,	0	9eu	0	0	0	0	8,	0	8eg	4	13	25	0.00040	237.4533	0.32

Note: the number of selected lines #, J_{min}, and J_{max} concerns the L.-S. fit in the global analysis. Sigma is the estimated uncertainty (one σ, in cm^{-1}) for unblended lines. Band cent. is the approximate band center (cm^{-1}), see text. Intens. is the maximum line intensity ($cm^{-2}\ atm^{-1} \times 10^3$) reached in the subband.

power series in $J(J+1)$ was not adequate for high J values of some states, so their data were only partly used. The two sets of data are in agreement within less than 0.0001 cm^{-1}.

4. Global rovibrational analysis

4.1. Principle

The global rovibrational analysis is based on an effective Hamiltonian for linear molecules as defined by Yamada et al. [26]. We take into account explicitly all rotational and vibrational ℓ-type resonances and some anharmonic and Coriolis resonances, and we fit simultaneously all polyads on the basis of a single set of molecular parameters. This procedure is explained in detail for penta-atomic molecules like HCCCN [27] and HCCNC [28], and the version adapted for six atomic molecules is described in Ref. [29]. We use for C_2N_2 the version for tetra-atomic molecules which has been applied for many years to acetylene C_2H_2 [30] and its ^{13}C [31] and deuterated isotopic species [32].

We develop the diagonal part of the Hamiltonian, (ω_i,x_{ij},$x_{\ell_i\ell_j}$,y_{ijk},...) for the vibration, (B,α_i,γ_{ij},$\gamma_{\ell_i\ell_j}$, ε_{ijk},...,D, β_i,β_{ij},...) for the rotation, as far as needed to reproduce

Table 2
Summary of the assigned sub-bands in the ν_4–ν_5 band of NCCN. Note that the band center of the subband reaching the $2\nu_4^0$ substate is shifted up by about 16 cm^{-1} by the anharmonic resonance with the ν_2 state.

Upper state							Lower state							#	J_{min}	J_{max}	Sigma	Band cent.	Intens.
0	0	0	1	0,	1	0eg	0	0	0	0	1,	0	1eu	18	4	64	0.00010	269.0518	2.56
0	0	0	1	0,	1	0fg	0	0	0	0	1,	0	1fu	20	4	67	0.00010	269.0518	2.55
0	0	0	1	1,	1	−1eu	0	0	0	0	2,	0	0eg	20	11	65	0.00010	270.1484	1.66
0	0	0	1	1,	1	1eu	0	0	0	0	2,	0	2eg	23	6	61	0.00010	268.5709	1.61
0	0	0	1	1,	1	1fu	0	0	0	0	2,	0	2fg	21	8	56	0.00010	268.5709	1.55
0	0	0	1	1,	1	1fu	0	0	0	0	2,	0	2eg	1	2	2	0.00040	268.5709	0.33
0	0	0	1	2,	1	0eg	0	0	0	0	3,	0	1eu	16	6	52	0.00020	269.9138	0.75
0	0	0	1	2,	1	0fg	0	0	0	0	3,	0	1fu	18	7	51	0.00020	269.9138	0.73
0	0	0	1	2,	1	2eg	0	0	0	0	3,	0	3eu	10	15	38	0.00020	268.0957	0.76
0	0	0	1	2,	1	2fg	0	0	0	0	3,	0	3fu	12	16	63	0.00020	268.0956	0.76
0	0	0	2	0,	2	0eg	0	0	0	1	1,	1	1eu	16	7	38	0.00020	269.7080	0.44
0	0	0	2	0,	2	0fg	0	0	0	1	1,	1	1fu	16	7	30	0.00020	269.7080	0.42
0	0	0	2	0,	0	0eg	0	0	0	1	1,	1	−1eu	21	12	46	0.00040	285.8083	0.43
0	0	0	1	3,	1	−1eu	0	0	0	0	4,	0	0eg	7	11	41	0.00040	270.5524	0.35
0	0	0	1	3,	1	1eu	0	0	0	0	4,	0	2eg	6	15	43	0.00060	269.4231	0.31
0	0	0	1	3,	1	1fu	0	0	0	0	4,	0	2fg	6	10	32	0.00040	269.4230	0.31
0	0	0	1	3,	1	3eu	0	0	0	0	4,	0	4eg	10	13	43	0.00020	267.6260	0.32
0	0	0	1	3,	1	3fu	0	0	0	0	4,	0	4fg	10	12	44	0.00020	267.6260	0.32
0	0	0	2	1,	2	1eu	0	0	0	1	2,	1	2eg	13	17	53	0.00030	269.2210	0.28
0	0	0	2	1,	2	1fu	0	0	0	1	2,	1	2fg	10	18	50	0.00030	269.2211	0.28

Note: see footnote to Table 1.

Table 3
Summary of assigned sub-bands in the ν_5 band system of N^{13}CCN and ^{15}NCCN, from present work and from Grecu's work [25].

Upper state							Lower state							#	J_{min}	J_{max}	Sigma	Band cent.	Intens.
N^{13}CCN																			
0	0	0	0	1,	0	1e	0	0	0	0	0,	0	0e	27	4	78	0.00010	231.1718	5.69
0	0	0	0	1,	0	1e	0	0	0	0	0,	0	0e	34	4	86	0.00010	231.1718	[25]
0	0	0	0	1,	0	1f	0	0	0	0	0,	0	0e	13	3	64	0.00010	231.1718	10.13
0	0	0	0	1,	0	1f	0	0	0	0	0,	0	0e	14	5	70	0.00010	231.1718	[25]
0	0	0	0	2,	0	0e	0	0	0	0	1,	0	1e	22	11	68	0.00020	228.7778	1.93
0	0	0	0	2,	0	0e	0	0	0	0	1,	0	1e	32	4	81	0.00020	228.7778	[25]
0	0	0	0	2,	0	0e	0	0	0	0	1,	0	1f	8	13	46	0.00040	228.7778	2.93
0	0	0	0	2,	0	0e	0	0	0	0	1,	0	1f	11	5	55	0.00020	228.7778	[25]
0	0	0	0	2,	0	2e	0	0	0	0	1,	0	1e	19	17	66	0.00020	231.6229	1.83
0	0	0	0	2,	0	2e	0	0	0	0	1,	0	1e	24	4	61	0.00020	231.6229	[25]
0	0	0	0	2,	0	2e	0	0	0	0	1,	0	1f	12	8	59	0.00040	231.6229	3.66
0	0	0	0	2,	0	2f	0	0	0	0	1,	0	1f	20	11	64	0.00020	231.6229	2.00
0	0	0	0	2,	0	2f	0	0	0	0	1,	0	1f	28	4	71	0.00010	231.6229	[25]
0	0	0	0	2,	0	2f	0	0	0	0	1,	0	1e	13	8	55	0.00040	231.6229	3.29
0	0	0	0	3,	0	1e	0	0	0	0	2,	0	0e	25	7	62	0.00020	229.3046	1.26
0	0	0	0	3,	0	1f	0	0	0	0	2,	0	0e	12	3	47	0.00040	229.3045	2.03
0	0	0	0	3,	0	3e	0	0	0	0	2,	0	2e	19	13	47	0.00040	232.0742	1.03
0	0	0	0	3,	0	3e	0	0	0	0	2,	0	2f	7	7	48	0.00040	232.0742	1.63
0	0	0	0	3,	0	3f	0	0	0	0	2,	0	2f	13	13	52	0.00040	232.0742	1.03
0	0	0	0	3,	0	3f	0	0	0	0	2,	0	2e	8	8	38	0.00040	232.0742	1.64
0	1	0	0	0,	0	0e	0	0	0	0	1,	0	1e	22	4	56	0.00010	609.0720	[25]
0	1	0	0	0,	0	0e	0	0	0	0	1,	0	1f	12	5	60	0.00010	609.0720	[25]
^{15}NCCN																			
0	0	0	0	1,	0	1e	0	0	0	0	0,	0	0e	46	4	70	0.00040	231.9348	1.86
0	0	0	0	1,	0	1e	0	0	0	0	0,	0	0e	32	4	81	0.00010	231.9348	[25]
0	0	0	0	1,	0	1f	0	0	0	0	0,	0	0e	13	8	53	0.00040	231.9348	3.31
0	0	0	0	1,	0	1f	0	0	0	0	0,	0	0e	16	5	80	0.00020	231.9348	[25]
0	0	0	0	2,	0	0e	0	0	0	0	1,	0	1e	14	19	53	0.00040	229.2862	0.62

Table 3 (*continued*)

Upper state							Lower state							#	J_{min}	J_{max}	Sigma	Band cent.	Intens.
0	0	0	0	2,	0	0e	0	0	0	0	1,	0	1e	28	4	71	0.00020	229.2862	[25]
0	0	0	0	2,	0	0e	0	0	0	0	1,	0	1f	6	10	47	0.00060	229.2862	0.96
0	0	0	0	2,	0	2e	0	0	0	0	1,	0	1e	18	14	50	0.00040	232.3981	0.60
0	0	0	0	2,	0	2e	0	0	0	0	1,	0	1e	28	4	71	0.00020	232.3981	[25]
0	0	0	0	2,	0	2e	0	0	0	0	1,	0	1f	9	7	53	0.00040	232.3981	1.18
0	0	0	0	2,	0	2f	0	0	0	0	1,	0	1f	27	12	49	0.00040	232.3981	0.65
0	0	0	0	2,	0	2f	0	0	0	0	1,	0	1f	32	4	81	0.00010	232.3981	[25]
0	0	0	0	2,	0	2f	0	0	0	0	1,	0	1e	13	10	50	0.00020	232.3981	1.07
0	0	0	0	3,	0	1f	0	0	0	0	2,	0	0e	7	7	29	0.00040	229.8347	0.66
0	0	0	0	3,	0	3f	0	0	0	0	2,	0	2f	9	22	36	0.00060	232.8612	0.33
0	1	0	0	0,	0	0e	0	0	0	0	1,	0	1e	22	4	56	0.00010	603.8693	[25]
0	1	0	0	0,	0	0e	0	0	0	0	1,	0	1f	12	5	60	0.00010	603.8693	[25]

Note: see footnote to Table 1.

the data, but checking that all parameters have an acceptable order of magnitude. We introduce all parameters for rotational (q_i,$q_{i,j}$,q_i^J,...) and vibrational (r_{ij},$r_{ij,k}$,r_{ij}^J,...) ℓ-type resonances. Finally we choose the most important anharmonic (k_{ijk},k_{ijkl},...) and Coriolis (C_{ij},C_{ijk},...) resonances to be introduced, taking into account the order of the operators giving rise to those resonances and the expected energy difference between the levels in interaction. This choice will define the energy matrixes. Although the density of states is quite high for cyanogen, the number of resonances is rather limited, thanks to the fact that *g* and *u* states cannot interact with each other.

Diagonal and off-diagonal matrix elements considered in the global analyses of linear molecules, with the selected accidental resonances corresponding to HCCCN, are given in Appendix A of a paper about $HCCC^{15}N$ [33]. The index *s* is for an arbitrary mode, *n* for a non-degenerate stretching mode, and *t* for a degenerate bending mode. It is important to notice that we always use power series according to v_s, and not according to $(v_s+d_s/2)$ as many authors do. For cyanogen, two formulas had to be extended to higher orders in the power series according to v_s, the vibrational diagonal term up to the 5th order,

$$\begin{aligned}E_v^0 = &\sum_s \omega_s^0 v_s + \sum_{s\le s'} x_{ss'}^0 v_s v_{s'} + \sum_{t\le t'} x_{\ell_t\ell_{t'}}^0 \ell_t \ell_{t'} \\ &+ \sum_{s\le s'\le s''} y_{ss's''}^0 v_s v_{s'} v_{s''} + \sum_{s,t\le t'} y_{s\ell_t\ell_{t'}}^0 v_s \ell_t \ell_{t'} \\ &+ \sum_{s\le s'\le s''\le s'''} z_{ss's''s'''}^0 v_s v_{s'} v_{s''} v_{s'''} \\ &+ \sum_{s\le s',t\le t'} z_{ss'\ell_t\ell_{t'}}^0 v_s v_{s'} \ell_t \ell_{t'} \\ &+ \sum_{t\le t'\le t''\le t'''} z_{\ell_t\ell_{t'}\ell_{t''}\ell_{t'''}}^0 \ell_t \ell_{t'} \ell_{t''} \ell_{t'''} \\ &+ \sum_{s\le s'\le s''\le s'''\le s''''} w_{ss's''s'''s''''} v_s v_{s'} v_{s''} v_{s'''} v_{s''''} \\ &+ \sum_{s\le s'\le s'',t\le t'} w_{ss's''\ell_t\ell_{t'}} v_s v_{s'} v_{s''} \ell_t \ell_{t'} \\ &+ \sum_{s,t\le t'\le t''\le t'''} w_{s\ell_t\ell_{t'}\ell_{t''}\ell_{t'''}} v_s \ell_t \ell_{t'} \ell_{t''} \ell_{t'''}\end{aligned} \tag{1}$$

and the vibrational ℓ-type resonance coefficient up to the third order:

$$\begin{aligned}r_{tt'}^* = &r_{tt'}^0 + \sum_s r_{tt',s}^0 (v_s-\delta_{st}-\delta_{st'}) + \sum_{s\le s'} r_{tt',ss'}^0 (v_s-\delta_{st}-\delta_{st'}) \\ &\times (v_{s'}-\delta_{s't}-\delta_{s't'}) + \sum_{s\le s'\le s} r_{tt',ss's} (v_s-\delta_{st}-\delta_{st'}) \\ &\times (v_{s'}-\delta_{s't}-\delta_{s't'})(v_s-\delta_{st}-\delta_{st'}) \\ &+ \left[r_{tt'J}^0 + \sum_s r_{tt'J,s} (v_s-\delta_{st}-\delta_{st'})\right] J(J+1) + r_{tt'JJ} J^2 (J+1)^2\end{aligned} \tag{2}$$

where δ_{st} is the Kronecker symbol.

4.2. Model

The model used is defined by our choice of anharmonic and Coriolis interactions to be considered explicitly as off-diagonal terms rather than as contributions to diagonal terms in the frame of the perturbation theory. The Hamiltonian is developed as far as needed to reproduce the data, while checking that all parameters have an acceptable order of magnitude. All polyads are simultaneously fitted using a single set of molecular parameters.

The first vibrational states are v_5^u near 230 cm^{-1}, $(2v_5$ and $v_4)^g$ near 500 cm^{-1}, and $(3v_5$ and $v_4+v_5)^u$ near 700 cm^{-1}, and they seem to be isolated although we will show that the Coriolis interaction (C_{455}) between $2v_5$ and v_4 is weak but not fully negligible. The first important polyad consists of *g* states between 845 and 1020 cm^{-1}, and the corresponding scheme of interaction is illustrated in Fig. 4. Off-diagonal terms between parentheses correspond to interactions which are presently fixed to zero, but which could be free in the future on the basis of new or more accurate experimental data. Because anharmonic and Coriolis resonances are $\Delta k=0$ and $\Delta k=\pm 1$ interactions, respectively, the matrix is formed by two sub-matrices defined by the anharmonic interactions. The Coriolis terms appear to connect these sub-matrices, but they have negligible effects at low *J* values. As $\omega_2 \cong 2\omega_4 \cong 4\omega_5$, by analogy with C_2H_2 [34], polyads can be characterized

$\nu_4+2\nu_5$	C_{455}	C_{455}	(C_{2455})
	$2\nu_4$	(k_{445555})	k_{244}
		$4\nu_5$	k_{25555}
			ν_2

Fig. 4. The basic interaction scheme for NCCN illustrated by the $N_r=4$ polyad. Only the upper half of the symmetric matrix is detailed. The off-diagonal terms between parentheses correspond to interactions not yet introduced in our model.

by the pseudo-quantum number $N_r=4v_2+2v_4+v_5$ as far as we are not concerned with the v_1 and v_3 vibrational modes. The four interacting states correspond to 15 ℓ-substates, 9 in e-matrix and 6 in f-matrix, as illustrated in Fig. 5 by the corresponding reduced energies as a function of $J(J+1)$. The first order anharmonic interaction (or Fermi resonance) associated with k_{244} ($W_F=k_{244}/\sqrt{2}=$ 50.5(2) cm^{-1}) is by far the strongest resonance, with induced energy shifts of about ∓ 16.3 cm^{-1} for the v_2 and $2v_4^0$ states, whereas the $2v_4^2$ state is unperturbed. As far back as 1950, Langseth and Moller [35] proposed this interaction on the basis of the unusual relative positions of the Σ and Δ substates of $2v_4$ in their low resolution Raman spectra. Maki [36] gave the first estimate for the interaction energy.

When our assignments were reaching $v_5=4$ substates, we also had to consider in our global analysis the third order anharmonic interaction, associated with k_{25555} (≈ -0.45 cm^{-1}). The energy shifts do not exceed ∓ 0.005 cm^{-1} for the v_2 and $4v_5^0$ states, but the abnormal position of this Σ substate of $4v_5$, with respect to the corresponding Δ and Γ substates, can be perceived thanks to the high experimental accuracy. Furthermore, we take advantage of observing states up to $v_5=9$ where the interaction term is multiplied by a factor of almost 9 compared with $v_5=4$.

The fourth order anharmonic resonance between the Σ and Δ substates of the $2v_4$ and $4v_5$ states, associated with k_{445555}, is expected to be very small. This parameter was fixed to zero, but we think it could be determined later, when more data will be available about higher harmonics of v_4 and their combinations with v_5.

After introducing the k_{244} and k_{25555} anharmonic resonances, the agreement in the global analysis was always good for low J levels, but some systematic deviations were observed at increasing J values, particularly for some substates of v_4+2v_5. It became obvious (see Fig. 5) that the second order Coriolis interaction between v_4 and $2v_5$ had to be introduced in the model. There are two main parameters for this $\Delta k=\pm 1$ Coriolis resonance, C_{455} for the case ($\Delta\ell_4=\pm 1, \Delta\ell_5=0$) and C'_{455} for the case ($\Delta\ell_4=\mp 1, \Delta\ell_5=\pm 2$). We recall that all formulas are given in Appendix A of Ref. [33]. The effects of the third order Coriolis resonance between v_2 and v_4+2v_5 (Fig. 4) are expected to be negligible, and this interaction was not considered in the model. Table 4 presents the summary about polyads characterized by the pseudo-quantum

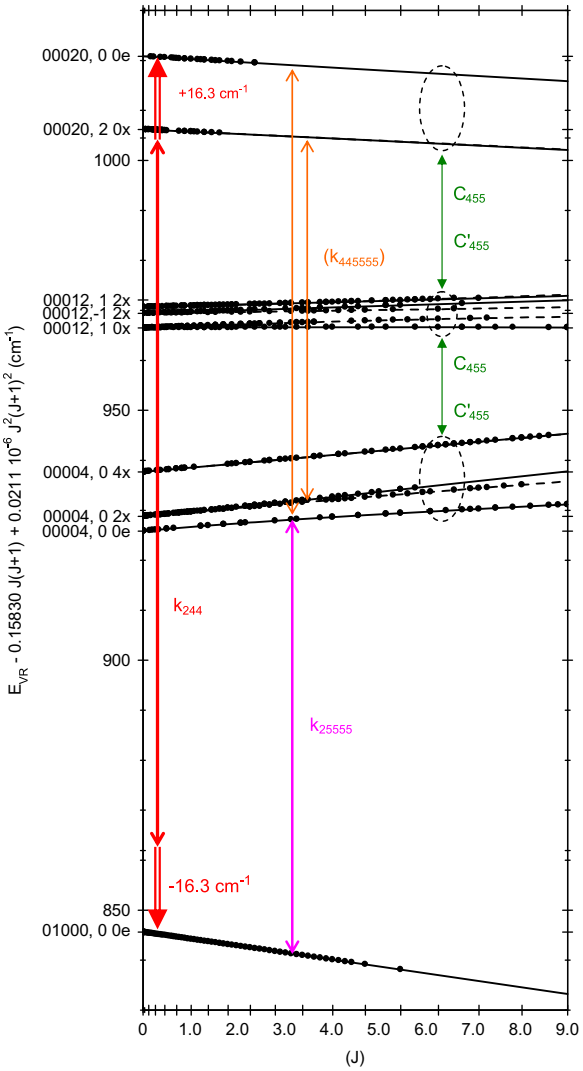

Fig. 5. Reduced rovibrational energies as a function of $J(J+1)$, for all ℓ-substates of NCCN between 830 and 1030 cm^{-1} corresponding to the $N_r=4$ g-polyad. The reduced energy (in cm^{-1}) corresponds to $E_{vr}-B_mJ(J+1)+D_0J^2(J+1)^2$, with the mean B value $B_m=0.1583$ cm^{-1} and the ground state centrifugal distortion constant $D_0=2.114\times 10^{-8}$ cm^{-1}. The states are identified in terms of $v_1v_2v_3v_4v_5,\ell_4\ell_5e/f$. The symbol x replacing e/f means that both components are quasi-degenerate at J_{min}. Components of e (f) symmetry are plotted in full (dotted) lines. Black circles correspond to upper levels of the selected observed transitions.

number $N_r=4v_2+2v_4+v_5$ from 0 to 10, as far as we are not concerned with the v_1 and v_3 vibrational modes.

4.3. The high resolution experimental data

The global analysis is limited to the numerous combinations of the v_5, v_4, and v_2 vibrational modes. Most experimental data come from the present work and we have to comment about the selection process of those data. Infrared bands contain between 20 and 200 lines. Thanks to the high coherence of the global analysis, we can reduce the number of experimental data in the global fit by

Table 4
NCCN polyads characterized by the pseudo-quantum number $N_r=4\nu_2+2\nu_4+\nu_5$ from 0 to 10, as long as we are not concerned with ν_1 and ν_3. States are classified according to decreasing ν_2 and ν_5 values, so that their energies are roughly in increasing order inside the polyad.

N_r	g/u	Energy range (cm^{-1})	# States	# e/f Substates	States
0	g	0	1	1	G.S.
1	u	234	1	1/1	ν_5
2	g	464–503	2	3/2	$2\nu_5$, ν_4
3	u	696–737	2	4/4	$3\nu_5$, $\nu_4+\nu_5$
4	g	845–1021	4	9/6	ν_2, $4\nu_5$, $\nu_4+2\nu_5$, $2\nu_4$
5	u	1083–1255	4	11/11	$\nu_2+\nu_5$, $5\nu_5$, $\nu_4+3\nu_5$, $2\nu_4+\nu_5$
6	g	1318–1538	6	19/16	$\nu_2+2\nu_5$, $\nu_2+\nu_4$, $6\nu_5$, $\nu_4+4\nu_5$, $2\nu_4+2\nu_5$, $3\nu_4$
7	u	1554–1771	6	24/24	$\nu_2+3\nu_5$, $\nu_2+\nu_4+\nu_5$, $7\nu_5$, $\nu_4+5\nu_5$, $2\nu_4+3\nu_5$, $3\nu_4+\nu_5$
8	g	1684–2065	9	38/32	$2\nu_2$, $\nu_2+4\nu_5$, $\nu_2+\nu_4+2\nu_5$, $\nu_2+2\nu_4$, $8\nu_5$, $\nu_4+6\nu_5$, $2\nu_4+4\nu_5$, $3\nu_4+2\nu_5$, $4\nu_4$
9	u	1926–2298	9	46/46	$2\nu_2+\nu_5$, $\nu_2+5\nu_5$, $\nu_2+\nu_4+3\nu_5$, $\nu_2+2\nu_4+\nu_5$, $9\nu_5$, $\nu_4+7\nu_5$, $2\nu_4+5\nu_5$, $3\nu_4+3\nu_5$, $4\nu_4+\nu_5$
10	g	2165–2590	12	67/60	$2\nu_2+2\nu_5$, $2\nu_2+\nu_4$, $\nu_2+6\nu_5$, $\nu_2+\nu_4+4\nu_5$, $\nu_2+2\nu_4+2\nu_5$, $\nu_2+3\nu_4$, $10\nu_5$, $\nu_4+8\nu_5$, $2\nu_4+6\nu_5$, $3\nu_4+4\nu_5$, $4\nu_4+2\nu_5$, $5\nu_4$

Table 5
Summary of complementary data for NCCN collected from the literature.

Upper state							Lower state							#	J_{min}	J_{max}	Sigma	Band cent.	Ref.
0	1	0	0	0,	0	0eg	0	0	0	0	0,	0	0eg	58	2	62	0.00050	845.5931	[7]
0	1	0	0	0,	0	0eg	0	0	0	0	1,	0	1eu	12	6	61	0.00010	611.8705	[25]
0	1	0	0	0,	0	0eg	0	0	0	0	1,	0	1fu	14	5	70	0.00010	611.8705	[25]
0	0	0	3	0,	3	0eg	0	0	0	0	0,	0	0eg	1	3	3	0.05000	1510.2448	[37]
0	0	0	3	0,	1	0eg	0	0	0	0	0,	0	0eg	1	1	1	0.05000	1537.0073	[37]
0	0	0	3	0,	1	0eg	0	0	0	1	0,	1	0eg	2	1	1	0.05000	1034.2329	[37]
0	0	0	3	0,	1	0eg	0	0	0	3	0,	3	0eg	1	3	3	0.05000	26.7625	[37]
0	2	0	0	0,	0	0eg	0	0	0	0	0,	0	0eg	2	0	0	0.50000	1684.7568	[4,38]
0	0	0	4	0,	4	0eg	0	0	0	0	0,	0	0eg	1	4	4	0.05000	2014.9366	[37]
0	0	0	4	0,	2	0eg	0	0	0	0	0,	0	0eg	1	2	2	0.05000	2052.1580	[37]
0	0	0	4	0,	2	0eg	0	0	0	2	0,	2	0eg	2	2	2	0.05000	1045.9679	[37]
0	0	0	4	0,	2	0eg	0	0	0	4	0,	4	0eg	1	4	4	0.05000	37.2214	[37]
0	0	0	4	0,	0	0eg	0	0	0	0	0,	0	0eg	1	0	0	0.05000	2064.5037	[37]
0	0	0	4	0,	0	0eg	0	0	0	2	0,	0	0eg	1	0	0	0.05000	1043.6785	[37]
0	0	0	4	0,	0	0eg	0	0	0	4	0,	2	0eg	1	2	2	0.05000	12.3457	[37]
0	1	0	2	2,	0	0eg	0	0	0	0	0,	0	0eg	1	0	0	0.07850	2318.5613	[39]
0	1	0	2	2,	0	2fg	0	0	0	0	0,	0	0eg	1	2	2	0.06400	2321.6156	[39]
0	1	0	2	3,	0	1eu	0	0	0	0	0,	0	0eg	1	1	1	0.00400	2553.5673	[39]
0	1	0	2	3,	0	3eu	0	0	0	0	0,	0	0eg	1	3	3	0.00370	2559.6103	[39]
0	1	0	2	4,	0	0eg	0	0	0	0	0,	0	0eg	1	0	0	0.00180	2786.0048	[39]
0	1	0	2	4,	0	2fg	0	0	0	0	0,	0	0eg	1	2	2	0.00120	2789.0371	[39]

Note: see footnote to Table 1.

introducing only some selected lines covering the observed range with a regular spacing in $J(J+1)$, according to a polynomial fit of the single band or, more frequently, selecting the lines by hand. In some cases (the cold band, very weak bands) we select almost all lines. In case of local perturbations, we select as many J's as needed to make use of the complete information available from the spectrum.

Although the ν_5 band system is measured around 230 cm^{-1}, the quality of the experimental spectrum and the ability to assign almost all experimental lines give access to upper substates as high in energy as 1912.1 cm^{-1} ($\nu_4^1+6\nu_5^6$) and 2120.3 cm^{-1} ($9\nu_5^9$), according to Table 1. For energies between 1500 and 2000 cm^{-1}, the assignments mainly depend on the intensity of the subbands. All substates under 1500 cm^{-1} have been reached by at least one subband, with two exceptions. The first one ($\nu_2+\nu_4^1$) is predicted at 1337.55 cm^{-1} but is not observed because the $\nu_2+\nu_4{}^1 \leftarrow \nu_2+\nu_5{}^1$ band is just too weak. The second one is ν_2 (845.59 cm^{-1}) to which no transition is expected in the measured range. However, this g state has been well determined from its Raman ν_2–G.S. band [7] and from its infrared ν_2–ν_5 band [25]. The summary of those data is listed in Table 5 with a few other complementary data collected from the literature. From the electronic spectra reported by Fish et al. [37], we have deduced informations about the $3\nu_4$ and $4\nu_4$ substates, with an estimated accuracy

of 0.05 cm^{-1}, important for the ν_4 mode parameters. The energy of the $2\nu_2$ state as proposed by Jones [4,38] is less accurate (0.5 cm^{-1}) but useful to estimate the x_{22} anharmonic parameter. Finally, from the local perturbations observed in the ν_1 band system of cyanogen and analyzed by Maki and Klee [39], we have estimated the unperturbed energies of most substates of $\nu_2+2\nu_4+2\nu_5$, $\nu_2+2\nu_4+3\nu_5$, and $\nu_2+2\nu_4+4\nu_5$ states, with an estimated accuracy between 0.08 and 0.001 cm^{-1}, data useful to determine high order vibrational parameters combining the three modes of interest.

4.4. Molecular parameters

We have obtained a statistical agreement with all experimental data, with an estimated standard deviation $\hat{\sigma}=0.806$ (as defined in Ref. [40]) close to unity, which shows that the fit is good and that the choice of the experimental uncertainties was correct. The largest deviations remain in the range of the experimental uncertainty (2.5σ), and the agreement is uniform according to J, without any systematic deviation at high J values.

The corresponding molecular parameters determined for the ν_2, ν_4, and ν_5 modes are listed in Table 6. In this table the names of the parameters are first given as they are printed from the global analysis program to avoid any transcription errors, and also using the classical notations according to the development of the effective Hamiltonian in Appendix A of Ref. [33]. All values are in agreement with their expected order of magnitude. They are given with enough digits to avoid any truncation problem in cases of high correlation between parameters. The highest correlations appear between the k_{244}, ω_2, x_{44}, $x_{\ell_4\ell_4}$, α_2, γ_{44}, and $\gamma_{\ell_4\ell_4}$ parameters. So x_{44} and $x_{\ell_4\ell_4}$ have exactly the same abnormally large uncertainty, which means that their sum is more accurate than the individual parameters. That is the reason why we consider x_{44} in spite of its large uncertainty. Our estimate of the interaction energy between ν_2 and $2\nu_4$ Σ states ($W_F=k_{244}/\sqrt{2}=50.53(19)\,cm^{-1}$) is expected to be more reliable than the previously published values, because we use more accurate data in a global analysis with no simplifying assumptions. Maki [36] proposed a first estimate at $\approx$ 44 cm^{-1}. In 1972, Fish et al. [37] obtained 51 ± 2 cm^{-1}. Jones proposed 49 cm^{-1} in 1973 [4] and 41.2 ± 1.0 cm^{-1} in 1974 [38]. More recently Maki et al. [8] estimated this interaction at 57.42 ± 0.25 and 51.08 ± 0.08 cm^{-1} for $^{15}NCC^{15}N$ and $N^{13}C^{13}CN$, respectively. The last value obtained by Maki in his very recent publication is 55.9 $\pm$ 0.1 cm^{-1}[9].

The sign of k_{244} has been arbitrarily chosen positive, and the same sign was first chosen for k_{25555}. When the global analysis was already well developed, we had systematic deviations at high J values, essentially in the lowest k-, highest ν_5-substates ($\nu_5^{\ell_5}=5^1$, 6^0, 7^1, and 8^0). The problem was directly solved by trying opposite signs for the two anharmonic interactions. The estimated standard deviation $\hat{\sigma}$ was reduced by 3%, the high J levels of the (00015, $1-1e$) substate, zero-weighted because unfitted, were perfectly predicted, and some high order parameters like $k_{25555,4}$ were reduced according to their expected order of magnitude. The explanation for this surprising observation is the bad choice of the sign of a purely vibrational resonance at the origin of systematic deviations clearly dependent on J and limited to a category of substates. On the basis of Figs. 4 and 5, the $2\nu_4$ and $4\nu_5$ states are indirectly coupled through the k_{244} and k_{25555} anharmonic resonances (the direct coupling via k_{445555} is probably negligible), with the ν_2 Σ as intermediate state. So this interaction will only influence the $\nu_5^{\ell_5}=4^0$, 5^1, $6^{0/2}$, $7^{1/3}\ldots$ substates. If the interaction term is roughly independent of J, its effect will be J-dependent because the rotational B constants of the interacting states are significantly different ($2\alpha_4=-72$ and $4\alpha_5=-215\times10^{-5}$ cm^{-1}). The energy calculations were independent of the signs of the Coriolis interaction parameters C_{455} and C'_{455}, so those parameters were chosen positive.

As pointed out by Botschwina [41], the *ab initio* calculated value (-1.30×10^{-15} cm^{-1}) for the equilibrium sextic centrifugal distortion constant H_e is very small for cyanogen, as also observed for cyanoacetylene [33], since the positive harmonic contribution is largely canceled by the negative Coriolis and anharmonic contributions. Without pure rotational spectra, on account of the symmetry of NCCN, the ground state parameters are determined by the ground state combination differences from any strong cold band (Table 7), but we can see that H_0 has never been determined in the previous works. Free in our global analysis, H_0 is not determined ($0.60\pm1.22\times10^{-15}$ cm^{-1}) but the order of magnitude is in agreement with *ab initio* values. Finally, H_0 has been kept free, but with a constraint at ($-1.30\pm0.13\times10^{-15}$ cm^{-1}) with a $\pm$10% interval to take into account the uncertainty of the *ab initio* value and the difference between H_e and H_0. At high J values, the parameters of the last line of Table 7 are recommended, with more decimal digits according to Table 6 because D_0 and H_0 are highly correlated. A last comment about H_5^0, the linear dependence of H_0 according to ν_5: it is well determined, with the same order of magnitude as H_0, a result of the abnormal smallness of H_0. This situation is similar to the case of H_7^0 for cyanoacetylene [33].

4.5. Effective state parameters

The molecular parameters of Table 6 as determined in the global least-squares procedure are used to calculate effective parameters for any substate. For all J values up to some J_{max} and for all polyads of interest, we first generate the calculated rovibrational energies by direct diagonalisation of the energy matrices. Next we fit the rovibrational energies of each substate to power series in $J(J+1)$ up to the sixth order and with a negative sign for the second order term. Thus we obtain the effective values of E_ν, B_ν, D_ν, H_ν, L_ν, M_ν, and N_ν, for all substates of NCCN up to 2150 cm^{-1}, available as Supplementary material and in good agreement with Maki [9]. For unperturbed states the higher order parameters are undetermined and they are fixed to zero. For heavily perturbed states the power series in $J(J+1)$ is no longer suitable for a good fit and the effective parameters are to be used with caution. The vibrational terms G_ν (cm^{-1}), calculated according to $G_\nu=E_\nu+B_\nu k^2+D_\nu k^4$, are also listed after the E_ν values.

Table 6
Molecular parameters of NCCN as determined by the global analysis for ν_2, ν_4, and ν_5. All values are in cm^{-1}.

Parameter		Value	Uncertainty	Factor
Vibrational diagonal parameters				
om2	ω_2	865.748803	0.221647	
om4	ω_4	502.453043	0.000059	
om5	ω_5	233.489615	0.000021	
x22	x_{22}	−4.110681	0.182842	
x24	x_{24}	2.600501	0.139755	
x25	x_{25}	4.519334	0.002211	
x44	x_{44}	−0.030426	0.033608	
x45	x_{45}	−0.417446	0.000062	
x55	x_{55}	−0.550334	0.000018	
xℓ4ℓ4	$x_{\ell_4\ell_4}$	0.509242	0.033605	
xℓ4ℓ5	$x_{\ell_4\ell_5}$	0.713918	0.000057	
xℓ5ℓ5	$x_{\ell_5\ell_5}$	0.940353	0.000014	
y245	y_{245}	−0.096219	0.006398	
y255	y_{255}	−0.099244	0.000111	
y445	y_{445}	0.002537	0.000578	
y455	y_{455}	0.001356	0.000029	
y555	y_{555}	0.011799	0.000009	
y2ℓ5ℓ5	$y_{2\ell_5\ell_5}$	0.040779	0.000078	
y4ℓ4ℓ5	$y_{4\ell_4\ell_5}$	0.000093	0.000042	
y4ℓ5ℓ5	$y_{4\ell_5\ell_5}$	0.002405	0.000027	
y5ℓ4ℓ4	$y_{5\ell_4\ell_4}$	−0.001475	0.000566	
y5ℓ4ℓ5	$y_{5\ell_4\ell_5}$	0.000659	0.000028	
y5ℓ5ℓ5	$y_{5\ell_5\ell_5}$	−0.011227	0.000009	
z2555	z_{2555}	1.949220	0.057008	$E-03$
z4555	z_{4555}	0.090149	0.002893	$E-03$
z5555	z_{5555}	−0.246597	0.002135	$E-03$
z25ℓ5ℓ5	$z_{25\ell_5\ell_5}$	−1.274629	0.047960	$E-03$
z45ℓ4ℓ5	$z_{45\ell_4\ell_5}$	1.141769	0.018019	$E-03$
z45ℓ5ℓ5	$z_{45\ell_5\ell_5}$	−0.092578	0.003143	$E-03$
z55ℓ4ℓ4	$z_{55\ell_4\ell_4}$	−0.849718	0.020674	$E-03$
z55ℓ4ℓ5	$z_{55\ell_4\ell_5}$	0.013377	0.002709	$E-03$
z55ℓ5ℓ5	$z_{55\ell_5\ell_5}$	0.240445	0.002305	$E-03$
zℓ4455	$z_{\ell_4\ell_4\ell_5\ell_5}$	−0.310274	0.019712	$E-03$
zℓ4555	$z_{\ell_4\ell_5\ell_5\ell_5}$	−0.015011	0.001628	$E-03$
w55,555	$w_{55,555}$	0.005035	0.000282	$E-03$
w555ℓ55	$w_{555\ell_5\ell_5}$	−0.005723	0.000497	$E-03$
w5ℓ5555	$w_{5\ell_5\ell_5\ell_5\ell_5}$	0.000930	0.000221	$E-03$
Rotational diagonal parameters				
B0	B_0	15,708.820362	0.006160	$E-05$
alpha2	α_2	38.760434	0.100940	$E-05$
alpha4	α_4	−36.074894	0.007845	$E-05$
alpha5	α_5	−53.844568	0.002032	$E-05$
gam25	γ_{25}	−0.823279	0.006918	$E-05$
gam44	γ_{44}	−0.838757	0.025656	$E-05$
gam45	γ_{45}	0.129956	0.003239	$E-05$
gam55	γ_{55}	−0.017728	0.000983	$E-05$
gℓ4ℓ4	$\gamma_{\ell_4\ell_4}$	0.744250	0.025555	$E-05$
gℓ4ℓ5	$\gamma_{\ell_4\ell_5}$	−0.100263	0.003641	$E-05$
gℓ5ℓ5	$\gamma_{\ell_5\ell_5}$	0.071906	0.000724	$E-05$
eps555	ε_{555}	0.018544	0.010058	$E-07$
eps5ℓ45	$\varepsilon_{5\ell_4\ell_5}$	1.096994	0.064843	$E-07$
eps5ℓ55	$\varepsilon_{5\ell_5\ell_5}$	−0.338160	0.014578	$E-07$
D0	D_0	2.113795	0.000547	$E-08$
beta2	β_2	0.026164	0.001329	$E-08$
beta4	β_4	0.047291	0.001126	$E-08$
beta5	β_5	0.095180	0.000326	$E-08$
beta25	β_{25}	−0.239355	0.100967	$E-10$
beta45	β_{45}	0.239496	0.035091	$E-10$
beta55	β_{55}	0.043328	0.006503	$E-10$
betaℓ55	$\beta_{\ell_5\ell_5}$	−0.038139	0.007604	$E-10$

Table 6 (*continued*)

Parameter		Value	Uncertainty	Factor
H0	H_0	−1.279003	0.129285	$E-15$
Hv5	H_5	2.462495	0.186944	$E-15$
Rotational ℓ-type resonances				
q4	q_4	−12.746966	0.002534	$E-05$
q4v4	$q_{4,4}$	−0.366676	0.043537	$E-05$
q4v5	$q_{4,5}$	−0.105889	0.000868	$E-05$
q4J	q_{4J}	0.924894	0.073880	$E-10$
q5	q_5	−22.280702	0.001256	$E-05$
q5v2	$q_{5,2}$	0.024601	0.002670	$E-05$
q5v4	$q_{5,4}$	−0.225224	0.003948	$E-05$
q5v5	$q_{5,5}$	−0.053393	0.001810	$E-05$
q5v45	$q_{5,45}$	−5.610789	0.783128	$E-08$
q5v55	$q_{5,55}$	0.878673	0.097707	$E-08$
q5J	q_{5J}	6.035196	0.039503	$E-10$
q5Jv4	$q_{5J,4}$	0.322555	0.053371	$E-10$
q5Jv5	$q_{5J,5}$	0.056417	0.007407	$E-10$
q5JJ	q_{5JJ}	−2.982691	0.314468	$E-15$
q445	q_{445}	−0.007377	0.002173	$E-05$
q455	q_{455}	−0.013411	0.000431	$E-05$
u45	u_{45}	0.115328	0.018175	$E-10$
u55	u_{55}	−0.028597	0.001267	$E-10$
Vibrational ℓ-type resonances				
r45	r_{45}	−0.665550	0.000019	
r45v2	$r_{45,2}$	5.025379	0.765101	$E-02$
r45v4	$r_{45,4}$	−1.316546	0.079487	$E-02$
r45v5	$r_{45,5}$	1.116839	0.003206	$E-02$
r45v55	$r_{45,55}$	−3.967875	0.182142	$E-04$
r45v555	$r_{45,555}$	11.439889	2.815050	$E-06$
r45J	r_{45J}	−0.052621	0.003442	$E-05$
r45Jv5	$r_{45J,5}$	0.266639	0.053060	$E-07$
r4455	r_{4455}	−1.069941	0.027130	$E-03$
Anharmonic resonances				
k244	k_{244}	71.462130	0.269255	
k244v2	$k_{244,2}$	−2.638448	0.142908	
k244v4	$k_{244,4}$	−0.562322	0.012267	
k244v5	$k_{244,5}$	−0.653956	0.008117	
k25,555	$k_{25,555}$	−0.452819	0.003367	
k25,555v4	$k_{25\ 555,4}$	0.034793	0.002977	
k25,555v5	$k_{25,555,5}$	0.006196	0.000247	
k25,555J	$k_{25,555J}$	0.308139	0.022745	$E-05$
Coriolis resonances				
C455	C_{455}	0.252206	0.033727	$E-03$
Cp455	C'_{455}	9.141359	0.026999	$E-03$
Cp455v4	$C'_{455,4}$	0.039194	0.009316	$E-03$
Cp455v5	$C'_{455,5}$	−0.037455	0.003116	$E-03$
Cp455J	C'_{455J}	−2.178975	0.204270	$E-08$

Table 7
Ground state parameters for NCCN, in cm^{-1}.

$B_0 \times 10^5$	$D_0 \times 10^8$	$H_0 \times 10^{15}$	Ref.	Basis
15,708.807(19)	2.1163(18)		[6]	ν_5 Band Table 3
15,708.769(14)	2.1106(16)		[6]	ν_5 Complex Table 4
15,708.809(7)	2.1155(8)		[39]	Various bands Table 2
15,708.807(19)	2.1163(18)		[25]	Table 3
15,708.829(6)	2.1158(5)		This work	ν_5 Complex
15,708.820(6)	2.1138(5)	−1.28(13)	This work	*Ab initio* [41] + ν_5 complex

The last two columns of this table give an estimate of the quality of the fit on the basis of the standard deviation of the fit (sigma, with a zero value if lower than 0.000005 cm^{-1}) and of the used J_{max} value. Normally $J_{max}=120$, but this J_{max} has been reduced automatically for too perturbed states, generally by the ℓ-type resonances. In cases where sigma is

large and/or J_{max} is reduced, any extrapolation above J_{max} should be very bad. The accuracy of the vibrational energies E_v can be estimated on the basis of the accuracy of the corresponding experimental data listed in Tables 1, 2, and 5. The coherence of the global analysis is expected to provide good predictions for unobserved substates, except for combinations of modes 2 and 4, and states with $v_2>1$ or $v_4>2$.

4.6. $N^{13}CCN$ and $^{15}NCCN$ isotopologues

We have started a global analysis of $N^{13}CCN$ and $^{15}NCCN$ isotopologues on the basis of the limited experimental data summarized in Table 3. Most parameters were fixed to their NCCN value (Table 6), but twenty of them were let free to fit the experimental data (see Table 8). We have obtained a statistical agreement uniform according to J for all experimental data, with an estimated standard deviation $\hat{\sigma}=0.76$ and 0.67 for $N^{13}CCN$ and $^{15}NCCN$, respectively.

5. Intensities

5.1. Theory

Our calculations of the relative intensities for linear molecules have been described in detail in two papers devoted to C_4N_2, about the v_9 band system [29] and the v_7+v_9 and $2v_7-v_9$ bands systems [42]. From now on, we will consider the absolute intensity of the transition or line strength (S_{abs} or simply S), on the basis of the same conventions and formulas. The relative intensity of a transition was given [29] by

$$S_{rel}=C\nu g e^{-(E/kT)}(1-e^{-(\nu/kT)})D^2 \tag{3}$$

The arbitrary factor C is to be replaced, using cgs units, by

$$\frac{8\pi^3}{3hc}L\frac{T_0}{T}\frac{1}{Q}C_i=11.1833\frac{T_0}{T}\frac{1}{Q}C_i \tag{4}$$

For a given temperature T(K), the line strength expressed in $cm^{-2}\,atm^{-1}$ is

$$S(cm^{-2}\,atm^{-1})=11.1833\frac{T_0}{T}\frac{1}{Q}C_i\sigma g e^{-(hcE_{vr}/kT)}(1-e^{-(hc\sigma/kT)})D^2 \tag{5}$$

$T_0=273.15$ K is the reference temperature for the Loschmidt number $L=2.68676\times10^{19}\,atm^{-1}\,cm^{-3}$, Q is the total partition function, C_i is the isotopic abundance of the considered species (0.9706, 0.02214, and 0.007243 for NCCN, $N^{13}CCN$, and $^{15}NCCN$ respectively, for natural cyanogen), $\sigma(cm^{-1})=E'_{vr}(cm^{-1})-E''_{vr}(cm^{-1})$ is the wavenumber of the transition, written ν in the previous papers, and g is the degeneracy of the lower state. The next two terms are the Boltzmann factor and the stimulated emission factor. As energies are given in cm^{-1}, the hc factor has been introduced explicitly in the two exponentials to clarify our notations. At last, the effective transition dipole moment D is given in units of Debyes.

The total degeneracy g may be factored in three terms: $g=g_{vib}\ g_{rot}\ g_{ns}$ The vibrational degeneracy is removed ($g_{vib}=1$) by the e/f separation in the symmetrized basis while the rotational degeneracy $g_{rot}=2J+1$ is included in the rotational part (Hönl–London factor) of the transition moment, so that, in this formula, the degeneracy only includes the nuclear statistical weight g_{ns}. The spin

Table 8
Global fit parameters and their standard-deviation (cm^{-1}) for the $N^{13}CCN$ and $^{15}NCCN$ isotopologues. All other parameters were fixed to their normal species value given in Table 6.

	$N^{13}CCN$			$^{15}NCCN$	
Parameter	Calc. value	Uncertainty	Factor	Calc. value	Uncertainty
om2	860.830502	0.186915		854.947228	0.191871
om4	494.916248	0.505535		499.870557	0.442864
om5	230.946370	0.000048		231.703098	0.000083
x55	−0.506098	0.000037		−0.568921	0.000075
xℓ5ℓ5	0.887853	0.000030		0.952991	0.000070
y555	0.010622	0.000010		0.011783	0.000023
yℓ5ℓ5	−0.010026	0.000012		−0.011275	0.000033
B0	15639.837744	0.022228	$E-05$	15233.941517	0.025365
alpha2	38.902426	0.160458	$E-05$	36.981067	0.131897
alpha5	−52.511758	0.002786	$E-05$	−52.216084	0.003072
gam55	−0.016769	0.000870	$E-05$	−0.018123	0.000874
gℓ5ℓ5	0.058417	0.001329	$E-05$	0.078607	0.001579
D0	2.106041	0.002722	$E-08$	1.982529	0.003244
beta2	0.026096	0.001167	$E-08$	0.023890	0.001124
beta5	0.093073	0.000397	$E-08$	0.090130	0.000437
q5	−22.330164	0.002338	$E-05$	−21.115338	0.002701
q5v5	−0.046473	0.001762	$E-05$	−0.055096	0.002323
q5J	6.095675	0.064458	$E-10$	5.623939	0.067412
k244	70.168650	0.375948		70.167401	0.439513
Cp455	9.023032	0.084030	$E-03$	8.851530	0.073690

statistics for NCCN is described in detail in Refs. [6,13], and the statistical weights for symmetric and antisymmetric nuclear spin wavefunctions ($g^s_{ns}:g^a_{ns}$) are (6:3). This symmetric/antisymmetric character can be determined according to the product $(x_{gu}x_{ef}x_J)=+1/-1$, respectively, with $x_{gu}=+1/-1$ for g/u states, $x_{ef}=+1/-1$ for e/f substates, and $x_J=+1/-1$ for even/odd J values. The nuclear statistical weights g_{ns} may be defined in different ways, keeping the same ratio g^s/g^a which corresponds to the intensity alternations observed in the infrared bands as illustrated in Fig. 4 of Ref. [25]. For the normal cyanogen, possible ratios are (6:3), (6/9 : 3/9), or (2:1). We have choosen to normalize the nuclear statistical weights g_{ns} by dividing them by half their sum and obtaining the ratio (4/3 : 2/3). The sum is then always equal to 2 like for the asymmetric species for which (1:1) is used. In that way, all isotopologues will have similar partition functions.

On the basis of the global analysis of NCCN, its total partition function Q has been calculated without any approximation by direct summation according to the relation:

$$Q=\sum_{all\ \ levels}(2J+1)\,g_{ns}\,e^{-(hcE_{vr}/kT)} \tag{6}$$

with J up to 130 and vibrational energies up to 3500 cm^{-1} to avoid any truncation error for temperatures up to 350 K. The total partition function is frequently factorized as $Q=Q_{vib}Q_{rot}$, with

$$Q_{vib}=\sum_{all\ \ substates}e^{-(hcE_v/kT)} \tag{7}$$

The vibrational energy E_v is the first term in the power series expansion in $J(J+1)$ of the rovibrational energies, as listed in the Supplementary material. Using the vibrational term G_v instead of E_v should reduce Q_{vib} by about 0.1%. We think that, at room temperature, the accuracy of the calculated Q and Q_{vib} partition functions is about 0.1%, and of course better at lower temperatures. The rotational partition function can be deduced with the same accuracy using $Q_{rot}=Q/Q_{vib}$. Total and vibrational partition functions of the main three isotopologues of cyanogen are listed in Table 9 for temperatures from 350 to 10 K, with an accuracy of about 1% for $N^{13}CCN$ and $^{15}NCCN$ species.

The general theory to calculate the transition dipole moment D and so the line intensities is explained in detail in Chapter 5 of Ref. [29] as well as its application to $\Delta v_t=+1$ transitions. The case of $\Delta v_t=\Delta v_{t'}=+1$ transitions is detailed in the paragraph 5.1 of Ref. [42], and we now follow exactly the same procedure for $\Delta v_t=-\Delta v_{t'}=+1$ transitions, to apply them to the v_4–v_5 band intensities. In the case of a two quanta transition of two degenerate modes $\Delta v_t=+1$, $\Delta v_{t'}=-1$, $\alpha=z$ and $\Delta K=0$ (parallel band), the unperturbed transition moments are given by

$$\begin{aligned}D^{\pm}&={}^{e/f}_{0}\langle v_i,v_t+1,\ell_t\pm1,v_{t'}-1,\ell_{t'}\mp1;J',\\&\quad k\Big|\frac{\partial^2\mu_z}{\partial q_t\partial q_{t'}}q_tq_{t'}\Phi_{Zz}\Big|v_i,v_t,\ell_t,v_{t'},\ell_{t'};J,k\rangle^{e/f}_0\\&=\mu_z^{tt'}D^{\pm}_{vt}D^{\pm}_{vt'}D_r\sqrt{2}\quad\text{for full−zero states and}\\&=\mu_z^{tt'}\left[D^{\pm}_{vt}D^{\pm}_{vt'}D_r(\pm)^sD^{\pm*}_{vt}D^{\pm*}_{vt'}D^*_r\right]\quad\text{in other cases.}\end{aligned} \tag{8}$$

The $D^{\pm*}_{vt}D^{\pm*}_{vt'}D^*_r$ term corresponds to the second contribution of Eq. (18) of Ref. [29] and μ corresponds to the vibrational transition moment.

The vibrational factors are

$$D^{\pm}_{vt}=\langle v_t+1,\ell_t\pm1|q_{t+}+q_{t-}|v_t,\ell_t\rangle=\mp\sqrt{(v_t\pm\ell_t+2)/2} \tag{9}$$

$$D^{\pm}_{vt'}=\langle v_{t'}-1,\ell_{t'}\mp1|q_{t'+}+q_{t'-}|v_{t'},\ell_{t'}\rangle=\mp\sqrt{(v_{t'}\pm\ell_{t'})/2} \tag{10}$$

and the rotational factor (or Hönl–London factors)

$$D_r=L_X(J,k) \tag{11}$$

with $X=R,P(e-e\text{ or }f-f),\text{or }Q(e-f\text{ or }f-e)$.

For the bands of the v_4–v_5 band system, the unperturbed transition moment is

$$\begin{aligned}D^{\pm}_X&={}^{e/f}_{0}\langle v_4+1,\ell_4\pm1,v_5-1,\ell_5\\&\quad\mp1;J',k|\mu_z^{45}q_4q_5\Phi_{Zz}|v_4,\ell_4,v_5,\ell_5;J,k\rangle^{e/f}_0\end{aligned} \tag{12}$$

and according to the considered branch:

$$\begin{aligned}D^{\pm}_R&=+\frac{1}{2}\mu_z^{45}\sqrt{(v_4\pm\ell_4+2)(v_5\pm\ell_5)}\\&\quad\times\sqrt{[(J+1)^2-k^2]/(J+1)}\{\sqrt{2}\}\end{aligned} \tag{13}$$

$$D^{\pm}_P=-\frac{1}{2}\mu_z^{45}\sqrt{(v_4\pm\ell_4+2)(v_5\pm\ell_5)}\sqrt{(J^2-k^2)/J}\{\sqrt{2}\} \tag{14}$$

$$\begin{aligned}D^{\pm}_Q&=+\frac{1}{2}\mu_z^{45}\ \sqrt{(v_4\pm\ell_4+2)(v_5\pm\ell_5)}k\\&\quad\times\sqrt{(2J+1)/J(J+1)}\{\sqrt{2}\}\end{aligned} \tag{15}$$

where $\{\sqrt{2}\}$ is the $\sqrt{2}$ factor in the particular case where one state (the upper or the lower one, but not both) is a "full-zero" state, according to Eq. (19) of Ref. [29].

5.2. Improved absolute intensities

In 1993, the Giessen group measured and analyzed the high resolution spectrum of the v_5 band system [6] and also carried out an evaluation of absolute line intensities [13] for the fundamental and for one hot band ($2v_5^{2e}-v_5^{1e}$), to determine the vibrational transition moment μ_x^5 and the nitrogen-broadening coefficient. Their measurements were carried out at $T=297.06$ K. The same temperature has been used here for our intensity calculations relative

Table 9
Total (Q) and vibrational (Q_{vib}) partition functions of cyanogen for temperatures from 350 to 10 K, for the main isotopologes NCCN, $N^{13}CCN$, and $^{15}NCCN$.

Temp. (K)	NCCN		$N^{13}CCN$		$^{15}NCCN$	
	Q	Q_{vib}	Q	Q_{vib}	Q	Q_{vib}
350.0	5476.97	3.55484	5624.01	3.63659	5722.18	3.60416
340.0	5040.23	3.36648	5172.12	3.44181	5263.63	3.41190
330.0	4633.98	3.18788	4751.99	3.25717	4837.24	3.22964
320.0	4256.44	3.01866	4361.75	3.08228	4441.11	3.05699
310.0	3905.90	2.85844	3999.59	2.91675	4073.43	2.89356
300.0	3580.70	2.70687	3663.82	2.76020	3732.46	2.73899
299.0	3549.52	2.69217	3631.63	2.74503	3699.77	2.72401
298.0	3518.57	2.67756	3599.68	2.72994	3667.33	2.70911
297.1	3490.92	2.66448	3571.14	2.71643	3638.34	2.69578
297.0	3487.86	2.66303	3567.98	2.71494	3635.14	2.69430
296.5	3472.59	2.65580	3552.22	2.70747	3619.13	2.68692
296.0	3457.38	2.64858	3536.53	2.70002	3603.19	2.67957
295.0	3427.13	2.63422	3505.31	2.68519	3571.48	2.66492
294.0	3397.11	2.61994	3474.33	2.67044	3540.02	2.65036
293.0	3367.32	2.60573	3443.59	2.65578	3508.80	2.63588
292.0	3337.76	2.59161	3413.09	2.64120	3477.82	2.62149
291.0	3308.42	2.57757	3382.82	2.62670	3447.08	2.60717
290.0	3279.31	2.56361	3352.79	2.61229	3416.57	2.59294
280.0	3000.23	2.42833	3064.96	2.47266	3124.18	2.45506
270.0	2742.06	2.30072	2798.85	2.34098	2853.79	2.32502
260.0	2503.45	2.18048	2553.05	2.21695	2603.99	2.20252
250.0	2283.13	2.06733	2326.25	2.10026	2373.43	2.08727
240.0	2076.55	1.96098	2117.17	1.99062	2160.84	1.97897
230.0	1889.23	1.86118	1924.61	1.88776	1964.98	1.87736
220.0	1716.75	1.76769	1747.43	1.79143	1784.73	1.78220
210.0	1558.07	1.68028	1584.56	1.70139	1618.97	1.69324
200.0	1412.22	1.59874	1434.98	1.61742	1466.68	1.61026
190.0	1278.25	1.52287	1297.71	1.53930	1326.88	1.53307
180.0	1155.30	1.45250	1171.83	1.46686	1198.63	1.46148
170.0	1042.52	1.38749	1056.49	1.39994	1081.06	1.39533
160.0	939.12	1.32769	950.84	1.33839	973.32	1.33448
150.0	844.35	1.27299	854.11	1.28209	874.63	1.27883
140.0	757.48	1.22334	765.56	1.23097	784.23	1.22829
130.0	677.84	1.17867	684.46	1.18497	701.40	1.18280
120.0	604.75	1.13897	610.13	1.14408	625.44	1.14236
110.0	537.58	1.10428	541.91	1.10831	555.67	1.10698
100.0	475.69	1.07464	479.14	1.07771	491.45	1.07672
90.0	418.44	1.05014	421.17	1.05236	432.09	1.05166
80.0	365.17	1.03082	367.32	1.03233	376.92	1.03186
70.0	315.20	1.01667	316.88	1.01758	325.22	1.01730
60.0	267.78	1.00741	269.08	1.00789	276.20	1.00774
50.0	222.10	1.00241	223.12	1.00259	229.04	1.00253
40.0	177.40	1.00045	178.19	1.00049	182.92	1.00048
30.0	133.08	1.00003	133.66	1.00003	137.21	1.00003
20.0	88.83	1.00000	89.22	1.00000	91.58	1.00000
10.0	44.58	1.00000	44.78	1.00000	45.96	1.00000

to Grecu's data. As pointed out by the authors, the rather high density of lines, provoking strong overlapping, was a problem for the intensity measurements. The best measurements were deduced from the NCCN spectra broadened with 8 mbar N_2. The final intensity fit was limited to 33 lines amongst the 68 measured lines, 45 in the cold band and 23 in the hot band, with experimental line intensities between 0.300 and 0.010 $cm^{-2}\,atm^{-1}$. On the other hand, in our high resolution spectra, we estimate that any line with intensity greater than 0.001 $cm^{-2}\,atm^{-1}$ and most lines in the 0.001–0.0002 $cm^{-2}\,atm^{-1}$ range could be assigned and fitted, or at least calculated with a frequency accuracy between 0.00005 and 0.001 cm^{-1}. A good estimation of their intensity was also obtained thanks to the high coherence of the global analysis. In order to take into account eventual overlapping or mixing lines that can be predicted by our calculations, we decided to correct the experimental line strengths [13] by a multiplying factor $S^{line}_{calc.}/\Sigma S^{mixed\ lines}_{calc.}$ (Table 10). The sum of mixed lines is calculated by considering the line strength of all the lines in a range of about $\pm 0.0015\,cm^{-1}$ around the main line frequency. We have found, among the 68 measured lines, correction factors ranging from 1 (no correction) to 0.37 for one strongly overlapped line but no correction factors lower than 0.92 among the 33 lines selected by Grecu for his final intensity fit. Nevertheless, the applied corrections were significantly reducing the dispersion of the experimental intensities, and the first evidence was an increase of intensities of about 6% at high J values, similar in both R- and P-branches of the cold band. We have therefore

Table 10
Correction of the experimental line strengths measured by Grecu [13] ($cm^{-2}\,atm^{-1}\times10^3$) on the basis of the calculated spectrum according to the global analysis of NCCN. The multiplying factor is defined as $S^{line}_{calc.}/\Sigma S^{mixed\ lines}_{calc.}$, and $m=J+1$ or $-J$ for R(J) or P(J) lines, respectively. Lines marked with s or w were not considered in the intensity analysis as explained in the text.

m	$S_{corr.}$		$S_{exp.}$
Cold band			
26	169.80		169.80 × 1.00
−27	136.80		138.50 × 0.99
−28	259.70	s	259.70 × 1.00
−29	135.80		146.00 × 0.93
31	314.30	s	330.80 × 0.95
34	157.50		157.50 × 1.00
35	292.70	s	292.70 × 1.00
36	153.68		159.30 × 0.96
−37	113.90		116.20 × 0.98
39	260.00	s	260.00 × 1.00
−41	100.90		103.10 × 0.98
43	234.10	s	237.60 × 0.99
45	212.80	s	212.80 × 1.00
−47	71.00		71.00 × 1.00
−48	138.40		138.40 × 1.00
−49	68.00		70.80 × 0.96
51	165.50		165.50 × 1.00
−53	54.60		56.20 × 0.97
−55	47.70		50.10 × 0.95
55	128.20		128.20 × 1.00
−56	88.60		92.30 × 0.96
57	115.90		115.90 × 1.00
58	54.80		58.30 × 0.94
−59	34.73		51.30 × 0.68
−60	64.70		67.40 × 0.96
62	40.80		41.30 × 0.99
−63	24.20		66.10 × 0.37
63	74.20		74.20 × 1.00
−64	38.90	w	38.90 × 1.00
64	34.40		35.10 × 0.98
65	64.20		64.20 × 1.00
−66	39.00		39.00 × 1.00
−67	16.95		20.50 × 0.83
67	54.10		55.80 × 0.97
−68	34.90		35.90 × 0.97
68	23.40	w	23.40 × 1.00
−70	27.80		28.70 × 0.97
71	39.63		39.90 × 0.99
−72	22.82		23.20 × 0.98
−73	10.70		11.00 × 0.97
−74	19.70		20.50 × 0.96
75	28.57		34.30 × 0.83
−78	12.90		13.60 × 0.95
79	17.70		17.90 × 0.99
81	15.00		15.00 × 1.00
Hot band			
17	53.87		59.30 × 0.91
18	105.00		116.00 × 0.90
19	56.52		58.00 × 0.97
20	114.60		117.40 × 0.98
21	55.56		55.90 × 0.99
22	108.96		114.90 × 0.95
23	54.80		54.80 × 1.00
26	109.80		119.40 × 0.92
−30	33.70		35.10 × 0.96
30	100.60		100.60 × 1.00
−31	65.20		65.20 × 1.00
32	91.28		93.30 × 0.98
−33	61.60		62.80 × 0.98
36	80.30		80.30 × 1.00
−38	30.56		33.30 × 0.92
42	67.23		68.00 × 0.99
−43	42.72		54.30 × 0.79
44	55.91		61.90 × 0.90
−45	28.50	w	28.50 × 1.00
46	56.94		59.90 × 0.95
47	21.69		23.20 × 0.94
−49	27.00		30.00 × 0.90
−50	11.00	w	11.00 × 1.00
50	37.80		37.80 × 1.00

introduced a Herman–Wallis factor:

$$F_{HW}=[1+c_2^{RP}m^2]^2\cong[1+2c_2^{RP}m^2] \text{ with } c_2^{RP}=5\pm1\times10^{-6}.$$

Using this factor, we have determined a vibrational transition moment coefficient $\mu_x^5=0.1795\pm0.0005D$ for the ν_5 band system, in perfect agreement with the values of Grecu et al. [13]; $0.1812\pm0.0019D$ for the cold band and $0.1790\pm0.0030D$ for the hot band. Fig. 6 illustrates the good general agreement of the improved experimental intensities with the calculated intensities for those two bands, and also the necessity of introducing the Herman–Wallis factor. We had however problems with some lines. First, we were surprised by a few lines observed at about 80% of their calculated intensity, whereas mixings are expected to increase their intensity. The common point for all those lines was the presence of an extra line of 10% to 20% of relative intensity and with a frequency shift in the 0.003–0.004 cm^{-1} range. This shift is too large to enhance the line, but we think it could enhance the base line and so reduce the determined experimental intensity. Those four lines are marked with a w in Table 10 and appear as down-triangles in Fig. 6. Second, the six strongest lines ($>0.200\,cm^{-2}\,atm^{-1}$) are systematically measured with intensities too low of about 3% to 9%, and we suspect small saturation effects. Those lines are marked with an s in Table 10 and appear as up-triangles in Fig. 6. The intensity fit was finally based on 58 of the 68 corrected lines, mainly on the 37 cold band lines because the 21 hot band lines present a slightly higher dispersion.

5.3. Intensity of the ν_4–ν_5 band

The introduction of the Coriolis resonance C_{455} between ν_4 and $2\nu_5$ indicates that these states belong to the same polyad. Some intensity transfer from the strong $2\nu_5^{0,\pm2}-\nu_5^{\pm1}$ perpendicular subbands to the $\nu_4^{\pm1}-\nu_5^{\pm1}$ parallel subbands is expected, but this mixing and the induced intensity transfer are expected to be extremely weak. For intensity calculations, we have to introduce two vibrational transition moment coefficients, μ_x^5 and μ_z^{45}, corresponding, respectively, to the $\Delta\nu_5=+1$ and $\Delta\nu_4=-\Delta\nu_5=+1$ selection rules. In a first approach, we have estimated the absolute intensity of a few P lines (m between −25 and −21) of the e–e and f–f components of the ν_4–ν_5 band in the 261 to 263 cm^{-1} region, by comparing with similar perfectly known lines of the ν_5 band. Surprisingly, using the determined μ_z^{45} ($0.027D$), the corresponding calculated R-branch appeared too strong

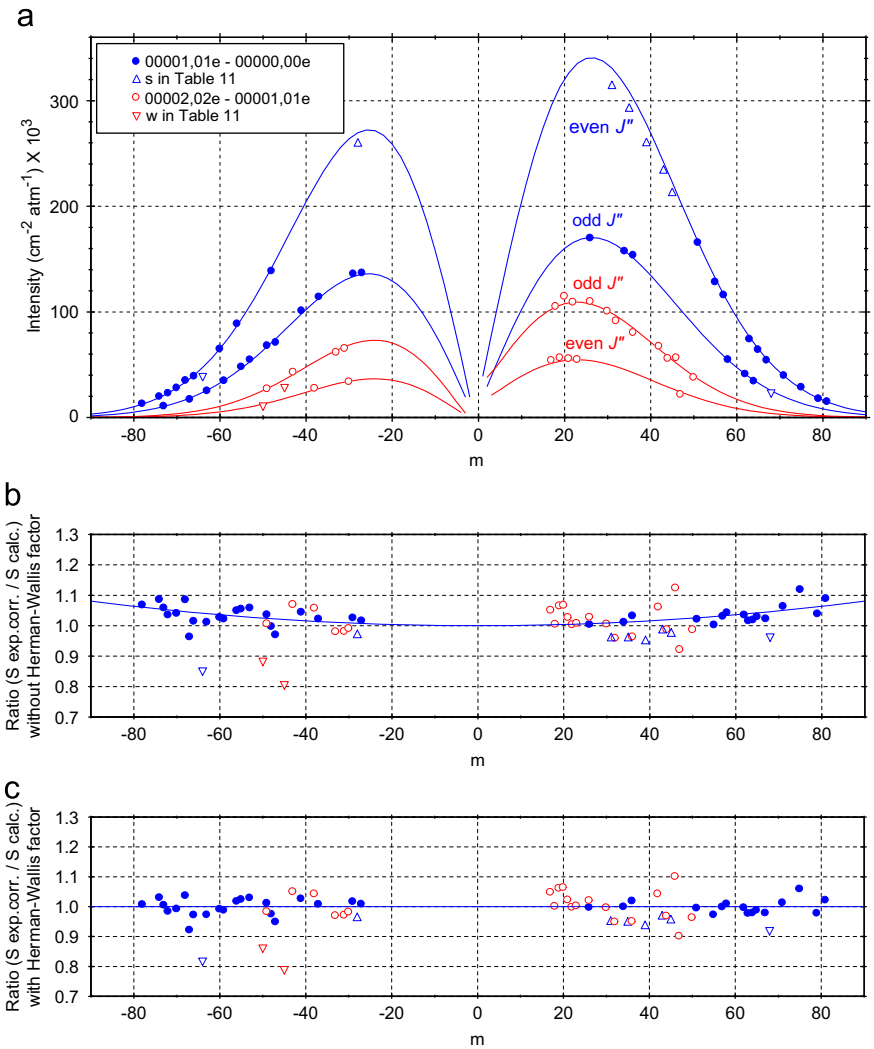

Fig. 6. Improved experimental ($S_{exp.corr}$, marks) and calculated ($S_{calc.}$, curves) line intensities ($cm^{-2}\,atm^{-1} \times 10^3$) for both subbands of NCCN used to determine the vibrational transition moment coefficient μ_x^5 for the ν_5 band system (part a). Ratios are given in parts b and c. From this analysis, essentially based on the 37 lines (full circles) of the cold band and confirmed by the 21 lines (empty circles) of the hot band, we have determined the vibrational transition moment coefficient $\mu_x^5 = 0.1795 \pm 0.0005D$ and the Herman–Wallis coefficient $c_2^{RP} = 5 \pm 1 \times 10^{-6}$. Other marks are explained in the text.

by about a factor two, comparing to both high and low resolution experimental spectra. The problem was solved by changing the sign of μ_z^{45}, but changing the sign of μ_x^5 or the sign of the Coriolis terms C'_{455} yields the same result. On the other hand, we could use the perfect linear relation between the absorbance and the intensity for the weakest lines ($S < 0.003\ cm^{-2}\ atm^{-1}$) of the ν_5 band. Applying the same proportionality to all lines of the ν_4–ν_5 band, we obtained a good estimate of the absolute intensity of 57 unblended lines in the *e–e* and *f–f* components of this band, from $P(59)$ to $R(61)$. Those experimental intensities are compared with different sets of calculated intensities in Fig. 7. First we illustrate the negligible intensity transfer from the Coriolis interaction in the case where $\mu_z^{45} = 0$. If the Coriolis term is fixed to zero, intensities (long-dashed curves) appear to be quite regular with a stronger R branch by about 14% compared to the P branch, and they are independent of the sign of the transition moment. In the present analysis, the μ_z^{45} transition moment is the main source of intensity, but those intensities are significantly influenced by the very weak Coriolis coupling, and this effect depends on the relative signs of the μ_x^5 and μ_z^{45} transition moments. With the same sign (dashed curves), the R branch exceeds the P branch by as much as 50%. On the contrary, with opposite signs (continuous curves), the R branch is weaker than the P branch by 14%, and this corresponds exactly to the experimental intensities for $\mu_z^{45} = -0.0253 \pm 0.0010D$.

5.4. Calculated spectrum

On the basis of the molecular parameters determined by the global analysis and of the intensity parameters (μ_x^5 with c_2^{RP}, and μ_z^{45}) determined in the two previous

paragraphs, we were able to generate automatically a line list of cyanogen in the 195–310 cm^{-1} spectral range. Details about this procedure can be found in two papers devoted to C_4N_2 spectra [29,42]. As our Hamiltonian includes all vibrational and rotational resonances which induce mixing of substates, the intensity calculations are good in all cases. For the wavenumbers, the accuracy is between 0.00005 and 0.001 cm^{-1} for transitions to observed substates. For most other transitions (very weak hot bands), we estimate the accuracy between 0.001 and 0.1 cm^{-1}.

Details about the absolute intensity results are listed in Table 11. The cold band includes 389 lines and accounts for only 25.6% of the overall band intensity of the normal isotope at room temperature. The first group of hot bands, from the $N_r=1$ polyad (ν_5), contains the strong $2\nu_5-\nu_5$ hot subbands and also the weak $\nu_4-\nu_5$, with intensities 37.513 and 0.303 $cm^{-2}\,atm^{-1}$, respectively. This illustrates the marginal character of the $\nu_4-\nu_5$ difference band compared to the ν_5 fundamental band. In this table, the second column, which indicates the number of substates, is underestimated by almost a factor two because, for a given upper substate, only one subband is counted even if there are two (*e* and *f*) lower substates. Considering higher N_r values, the number of subbands and the number of lines rapidly increase. This fact, combined with the significant increase of the vibrational factor with ν_5 and ℓ_5 values, partly compensates the decreasing Boltzmann factor so that hot bands up to $N_r=10-9$ (lower states up to about 2300 cm^{-1}) have to be considered to reach a 0.2% accuracy in our intensity calculations. The summed intensity for the normal NCCN band system is equal to 152.691 $cm^{-2}\,atm^{-1}$ and the contribution of $\Delta\nu_4=-\Delta\nu_5=+1$ transitions corresponds only to 0.77% of the total intensity (1.230 $cm^{-2}\,atm^{-1}$). In the second part of Table 11, we give the contributions of $N^{13}CCN$ and $^{15}NCCN$ calculated up to $N_r=7-6$ (lower states up to about 1500 cm^{-1}), assuming the same intensity parameters (the case of $^{15}NCCN$ is discussed below) as for the normal species. The sum of intensities of all bands of the three main isotopologues corresponds to a calculated integrated band intensity of 157.1 ± 1.0 $cm^{-2}\,atm^{-1}$. Finally, the lower part of Table 11 justifies the very low intensity threshold (0.000003 $cm^{-2}\,atm^{-1}$) required for room temperature spectra calculations. In the lower panel of Fig. 1, a comparison between a calculated spectrum using this new line list and our high resolution spectrum shows a very good agreement even for the very small features which are well reproduced by the model. This new line list containing 196,994 lines is available from the

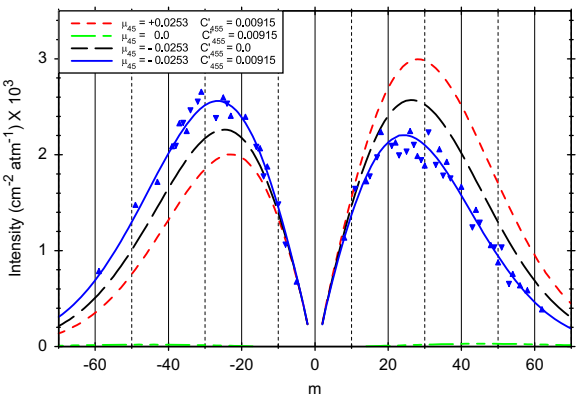

Fig. 7. Experimental (marks) and calculated (curves) line intensities ($cm^{-2}\,atm^{-1}\times10^3$) of the $\nu_4-\nu_5$ band of NCCN used to determine the corresponding vibrational transition moment coefficient $\mu_z^{45}=-0.0253\pm0.0010D$. Up- and down-triangles correspond, respectively, to *e*–*e* and *f*–*f* components of this band. As explained in the text, the different curves correspond to different hypotheses about the model or the parameters.

Table 11
Contributions of the different groups of subbands of NCCN and of the ^{13}C and ^{15}N isotopic species to intensities (in $cm^{-2}\,atm^{-1}$) of the ν_5 system of cyanogen at 296.5 K. The states belonging to the different N_r polyads are listed in Table 4. The lower part of the table justifies the very low intensity threshold (0.000003 $cm^{-2}\,atm^{-1}$) required for room temperature spectra calculations.

	# Subbands	# Lines	Intensity	%	Sum of intensities	%
NCCN—ν_5 band						
Cold band $N_r=1-0$	2	389	39.145	25.64	39.145	25.64
Hot bands $N_r=2-1$	5	1692	37.816	24.77	76.961	50.40
$N_r=3-2$	19	4396	31.099	20.37	108.060	70.77
$N_r=4-3$	35	8745	19.630	12.85	127.690	83.63
$N_r=5-4$	70	13485	12.076	7.91	139.766	91.54
$N_r=6-5$	101	18718	6.594	4.32	146.360	95.85
$N_r=7-6$	143	23553	3.476	2.27	149.836	98.13
$N_r=8-7$	190	26116	1.699	1.11	151.535	99.24
$N_r=9-8$	253	26793	0.805	0.53	152.340	99.77
$N_r=10-9$	307	23451	0.351	0.23	152.691	100.00
NCCN—ν_5 complex						
NCCN—ν_5 band	1127	147338			152.691	100.00
$N^{13}CCN$—ν_5 band band	204	30126			3.340	2.19
$^{15}NCCN$—ν_5 band	154	19530			1.077	0.71
Total	1485	196994			157.108	102.90
ν_5 Complex intensity threshold						
0.000003		196994			157.108	100.00
0.000030		82494			155.878	99.22
0.000300		25193			150.369	95.71

authors and will in the next update replace the 2298 lines presently available in the GEISA 2009 database [43].

5.5. Intensities in low resolution spectra

As presented in Section 2, low resolution spectra have been measured for both NCCN and ^{15}NCCN. Those spectra have been used to determine integrated band intensities and also to compare with calculated spectra using the new line list. A first comparison is shown in Fig. 8 where the contribution of hot bands is calculated for low resolution (0.5 cm^{-1}) spectra of natural cyanogen at room temperature (296.5 K) as a function of the maximum energy E'' of the considered lower vibrational states. The curve with the least absorbance in the graph ($E''=0$) corresponds to the cold band and accounts for only 25.6% of the overall band intensity. In the following curves ($E''<300$, 600, and 800 cm^{-1}) the contributions of hot bands, respectively, with lower states ν_5, ($2\nu_5$, ν_4), and ($3\nu_5$, $\nu_4+\nu_5$) are added and strong Q-branches at, respectively, 231.3, 228.8, and 226.4 cm^{-1} are observed. The contribution of hot bands from lower states ν_2, $4\nu_5$, $\nu_4+2\nu_5$, $2\nu_4$ ($E''<1050$ cm^{-1}) still adds more intensity and a weak feature at 224.1 cm^{-1}. Introducing the remaining hot bands together with the isotopic bands, we finally obtain the final curve $E''<2300$ cm^{-1}. This last curve almost perfectly coincides with the experimental spectrum which has been shifted up by 0.2 to help the comparison. Note that no distinguishable features at the present resolution can be assigned to the N^{13}CCN and ^{15}NCCN monosubstituted cyanogen.

A second comparison is shown in Fig. 9 illustrating the high frequency side of the ν_5 band system measured at

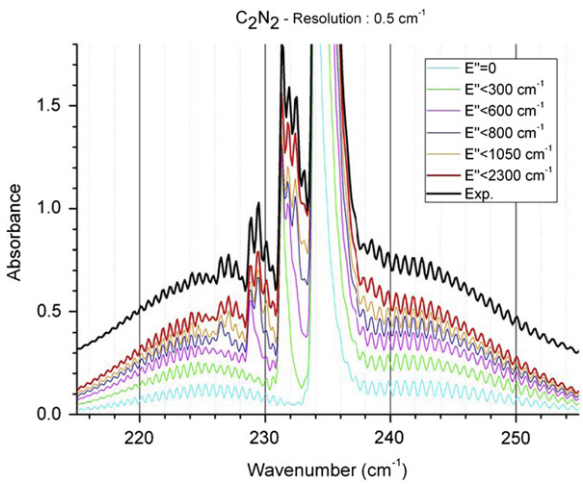

Fig. 8. Experimental spectra of the ν_5 band system of cyanogen taken at 0.5 cm^{-1} resolution and 296.5 K, compared to calculated spectra taking into account transitions arising from the ground vibrational states ($E''=0$) and progressively higher lying excited states ($E''<300$, 600, 800, 1050, 2300 cm^{-1}). The first five curves correspond to the progressive addition of the first five groups of subbands of Table 11, contributing to 25.6, 50.4, 70.8, 83.6, and 91.5% of the NCCN ν_5 band system intensity. The sixth curve includes all subbands of NCCN, N^{13}CCN, and ^{15}NCCN. The experimental spectrum has been shifted up by 0.2 to help the comparison.

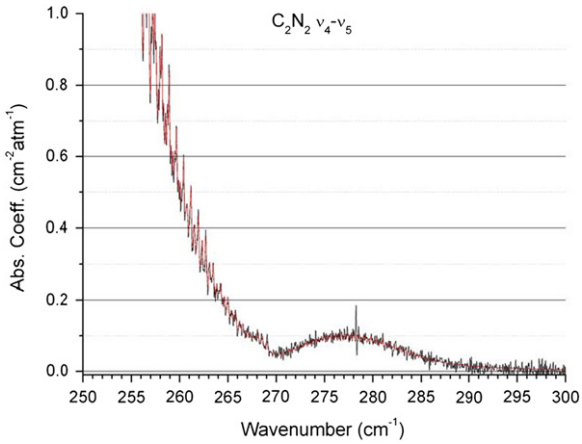

Fig. 9. High frequency side of the experimental spectrum of the ν_5 band of cyanogen taken at 0.1 cm^{-1} resolution and 296.5 K, showing the contribution of the $\nu_4-\nu_5$ difference band centered at 269.05 cm^{-1} and the excellent agreement with the calculated spectrum (in red). (For interpretation of the references to color in this figure legend, the reader is referred to the web version of this article.)

0.1 cm^{-1} resolution and showing the contribution of the R branch of the ν_4–ν_5 difference band. Despite the weak intensity of this band the agreement with the calculated spectrum is very good.

In addition to comparison with calculated spectra, low resolution experimental spectra have been used to measure integrated band intensities. For the normal C_2N_2, results have been obtained by averaging the 10 low resolution experimental spectra discussed in Section 2. The final result is 156.0 ± 2.5 cm^{-2} atm^{-1} at 296.5 K where the relatively small uncertainty can be justified by the limited spreading of the individual results. This result is in excellent agreement with the integrated band intensity of 157.1 ± 1.0 cm^{-2} atm^{-1} deduced from the correction made to the measured line intensities by Grecu et al. [13], as explained in Section 5.4 This agreement between line intensity measurement and integrated band intensity measurements demonstrates the high coherence of the intensity calculations based on the global analysis and also the high quality of the experimental measurements. Those results are also in good agreement with previous measurements of band intensities by Kim and King [11] who found 149.1 cm^{-2} atm^{-1} and Miyazawa [10] who found 152 cm^{-2} atm^{-1}. This demonstrates that the disagreement mentioned by Grecu et al. [13] between their line intensity measurements and Kim and King's [11] measurement is not real. As we will show below the discrepancy is probably due to the calculation of vibrational transition moment and not due to any experimental results.

Concerning ^{15}NCCN, integrated band intensities measured for the 6 low resolution experimental spectra at 296.5 K were averaged to obtain an experimental result of 149.5 ± 3.5 cm^{-2} atm^{-1} which is about 4% lower than the intensity of the normal species. The averaged spectrum of ^{15}NCCN is shown in Fig. 3 and compared to the averaged spectrum of NCCN. The intensity decrease of ^{15}NCCN compared to the normal isotopologue is, as expected,

very small. In the absence of any laboratory measurements, the intensities of isotopologues with one ^{15}N or one ^{13}C atom are usually taken to be unchanged as for HCN or C_2H_2 (see GEISA 2009 [43]) but in a few cases experimental results have shown significant decrease. This is the case of $HCCC^{15}N$ where a significant decrease of 15% has been measured [44]. Recently, we have also obtained a large decrease of 35% for the ν_8 band of $H^{13}CCCCH$ which could be explained by a strong perturbation due to the close lying ν_6 bending mode [15]. No such effect is observed here since we only observe a small intensity decrease, which is close to our precision limit.

5.6. Band intensity

Many authors have been using formulas to relate experimentally measured intensities to vibrational transition moment coefficients. Line intensities are obtained from Eq. (5) but band intensities and more specifically band system intensities are very often the only accessible measurements. Vibrational transition moment coefficients can still be obtained from such measurements if the proper relations are used.

The intensity of a band is given by summing the intensity of all the lines belonging to that particular band. A relation for the band intensity S_V^0 can also be obtained by simplifying all the rotational terms in Eq. (5) using relations (6) and (7) which enable to separate the vibrational and the rotational part:

$$S_V^0(\mathrm{cm^{-2}\,atm^{-1}}) = 11.1833\frac{T_0}{T}\frac{1}{Q_{vib}} C_i\sigma_0 e^{-(hcE_v/kT)}(1-e^{-(hc\sigma_0/kT)})D_{vib}^2 \quad (16)$$

In the case of the ν_5 band (or in any case where the selection rule is $\Delta\nu_t=+1$) the vibrational part D_{vib} of the transition moment can be written as the product of the constant term μ_x^5 and the vibrational factor $D_\nu^\pm = \mp\sqrt{(\nu_5 \pm \ell_5+2)/2}$ (see Ref. [29]):

$$D_{vib} = \mu_x^5\ D_\nu^\pm\{\sqrt{2}\} \quad (17)$$

where $\{\sqrt{2}\}$ is the $\sqrt{2}$ factor already evoked earlier which must be taken into account in the case of one full zero state. The S_V^0 value is an approximate value, since it is necessary to choose a central wavenumber σ_0 for the whole vibrational band. The induced emission term is also an averaged value dependent on the value of σ_0. This term is often omitted in the definition of the band intensity, which may be understandable in the case of the ν_5 band of acetylene where $e^{-(hc\sigma_0/kT)}=0.971$, but cannot be neglected in the case of lower lying vibrational modes, as the ν_5 band of cyanogen where $e^{-(hc\sigma_0/kT)}=0.679$. Finally the band intensity S_V^0 is the product of constant terms including the vibrational transition moment coefficient μ_x^5 and the vibrational factor which only depends on ν_5 and ℓ_5. It is thus possible to predict the unperturbed intensity of any hot band using Eqs. (16) and (17). As an example, we can calculate the intensity of the cold band of ν_5 in C_2N_2 using $\mu_x^5=0.1795D$ and $\sigma_0=234\,\mathrm{cm^{-1}}$. We find an intensity of $38.7\,\mathrm{cm^{-2}\,atm^{-1}}$ which is very close to the value obtained from the sum of line intensities reported in Table 11. Note that, in the case of this cold band, the vibrational factor is equal to $\sqrt{2}$, since the ground state is a full zero state, which introduces a factor of 2 in the calculation of the band intensity. Among the strongest hot bands, all three subbands in the $2\nu_5\leftarrow\nu_5$ hot band also have a squared vibrational factor of 2 but all four subbands in the $\nu_4+\nu_5\leftarrow\nu_4$ hot band have a factor of 1. This behavior has been observed experimentally by many authors studying the ν_5 band of acetylene. It is the case of Weber et al. [45] who finds a constant value for the ν_5 band system after introducing a factor 1/2 to all transitions belonging to $\nu_4+\nu_5\leftarrow\nu_4$. Other authors do not take into account any vibrational factor and obtain logically different values of μ_x^t for different hot bands [46]. Because of the different definitions that are used, μ_x^t values are not always comparable. Moreover, many authors take the vibrational factor of the cold band equal to one except Grecu et al. [13] who introduces a factor 2 called ω, equivalent to the "full-zero" state $\{\sqrt{2}\}$ factor described above. As a consequence, squared vibrational transition moment can change by a factor of two depending on the definition of the vibrational factors.

5.7. Band system intensity

Very often, low resolution experiments are only able to measure integrated intensities over the whole band system which includes all the hot bands and eventually the isotopic bands. It is nevertheless possible to determine a vibrational transition moment from such measurements. The intensity of the band system S_V^{BS} QUOTE is the sum of the intensity of all the vibrational bands of all unresolved isotopologues until the product of the isotopic abundance multiplied by the Boltzmann factor and by the squared vibrational factor becomes so small that their contribution to intensities reaches a fixed threshold value and can be neglected:

$$S_V^{BS} = \sum_{vib,iso} S_V^0 \quad (18)$$

The sum over all vibrational bands of all isotopologues is not straightforward but it can be calculated in the case of degenerate vibrational modes that

$$\sum_{vib,iso} C_i(1-e^{-(hc\sigma_0/kT)})\frac{e^{-(hcE_v/kT)}}{Q_{vib}}(D_\nu^\pm)^2 = 2 \quad (19)$$

This sum is relatively easy to calculate in the case of molecules such as HCN or C_2H_2, which have a reduced number of hot bands or for more complex molecules when the number of hot bands is reduced by low temperature conditions. Indeed, by reducing the temperature, all terms in Eq. (19) converge at some point to 1 except the isotopic abundance and the vibrational factor. Finally, the sum only consists of cold bands which have squared vibrational factors of 2 and the final result of the sum is inevitably 2. At room temperature and for molecules with a large number of hot bands, the number of terms in the sum becomes very important but we were able to calculate this sum for bending modes of C_2N_2,

HC_3N, and C_4H_2 and have as expected obtained a final sum equal to 2 with a dispersion lower than 0.5%. This factor seems thus essential for degenerate bending modes which have in common that the vibrational factor for the cold band is equal to 2.

All vibrational terms can thus be simplified and the band system intensity is finally given by

$$S_V^{BS}(\mathrm{cm}^{-2}\,\mathrm{atm}^{-1}) = 2 \times 11.1833 \frac{T_0}{T} \sigma_0 (\mu_x^5)^2 \tag{20}$$

Applying this relation to the case of the ν_5 band system of cyanogen using $\sigma_0 = 234\,\mathrm{cm}^{-1}$ and $\mu_x^5 = 0.1795D$ we obtain $S_V^{BS} = 155.78\,\mathrm{cm}^{-2}\,\mathrm{atm}^{-1}$, in very good agreement with the value obtained by summing the intensity of all the bands and reported in Table 11. Those relations differ by a factor 2 compared to relation (21) in Grecu et al. [13] and we think that this might be the reason why they have deduced a vibrational transition moment of 0.249 from Kim and King's [11] band system intensity measurement.

In conclusion, we have shown that line intensity and band system intensity measurements are in very good agreement and that comparison between both experimental studies can be made as long as proper relations are used.

6. Applications to Titan

The C_2N_2 line list that is used to analyze spectra of Titan's atmosphere can be found on the GEISA database. It contains 2577 lines, including lines belonging to the strongest hot bands. Corrections to the line list have been brought in the 2009 edition and concerned a number of hot sub-bands, which have been reduced by a factor 2 in intensity (see Jacquinet et al. [43]). This correction has already been taken into account by Teanby et al. [3] when retrieving the abundance of C_2N_2 in Titan's atmosphere from the latest CIRS far infrared observations. Teanby et al. [3] have detected for the first time C_2N_2 at equatorial and southern latitudes with an abundance of about 6×10^{-11}. They also confirm the strong enhancement of nitrile species at northern latitudes with a maximum C_2N_2 abundance of 3×10^{-9} in the north polar regions. This relatively large abundance at northern latitudes opens the way to the search for the isotopologues ^{15}NCCN and N^{13}CCN, which also benefit from the double C and N position in this molecule. As observed for HCN [16], ^{15}NCCN might also be enriched in Titan's atmosphere. For HCN, a ^{15}N/^{14}N equal to 1/56 has been determined and, taking into account the double N position in C_2N_2, this would result in a ^{15}NCCN/NCCN ratio of about 1/30 which means a possible ^{15}NCCN abundance of about 1×10^{-10}. Such abundance is already within reach of the CIRS detectors, but as can be seen in Fig. 10, a very high signal-to-noise ratio will be required to separate the contribution of various species. The new line lists for all three isotopologues are used to calculate individual spectra for each species and the sum of all three contributions taking normal abundance for N^{13}CCN and an enhanced abundance for ^{15}NCCN (Fig. 10). At the maximum CIRS resolution of 0.5 cm^{-1} bands belonging to both isotopologues overlap with each other and also with the strongest hot band. At the temperature of 160 K that has been chosen to mimic the conditions in the stratosphere of Titan, this hot band feature is still strong but, despite the overlap, the contribution of the isotopologues of C_2N_2 is not negligible and might be detected on Titan with the help of high quality observations with a good signal-to-noise ratio.

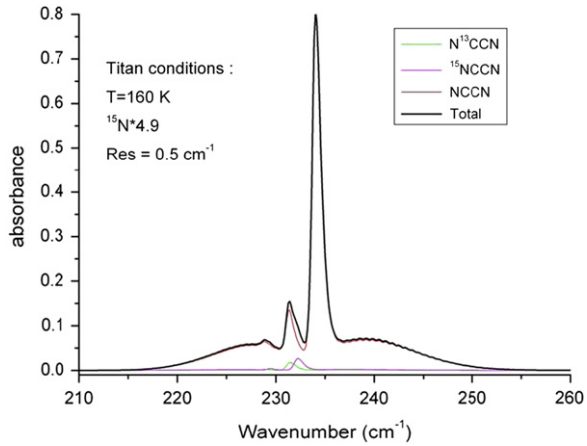

Fig. 10. Calculated spectra at 160 K for individual molecules (NCCN, ^{15}NCCN, and N^{13}CCN) and the total contribution of all isotopologues using natural abundances for N^{13}CCN and enhanced abundance (*4.9) for ^{15}NCCN.

Acknowledgments

One of the authors (AF) thanks for the computational resources provided by the supercomputing facilities of the Université catholique de Louvain (CISM/UCL) and the Consortium des Equipements de Calcul Intensif en Fédération Wallonie Bruxelles (CECI) funded by the Fond de la Recherche Scientifique de Belgique (FRS-FNRS).

Appendix A. Supplementary material

Supplementary data associated with this article can be found in the online version at doi:10.1016/j.jqsrt.2012.02.003.

References

[1] Kunde VG, Aikin AC, Hanel RA, Jennings DE, Maguire WC, Samuelson RE. C_4H_2, HC_3N and C_2N_2 in Titan's atmosphere. Nature 1981;292:686–8.
[2] Teanby NA, Irwin PGJ, de Kok R, Nixon CA, Coustenis A, Bezard B, et al. Latitudinal variations of HCN, HC_3N, and C_2N_2 in Titan's stratosphere derived from Cassini CIRS data. Icarus 2006;181:243–55.
[3] Teanby NA, Irwin PGJ, de Kok R, Jolly A, Bezard B, Nixon CA, et al. Titan's stratospheric C_2N_2, C_3H_4, and C_4H_2 abundances from Cassini/CIRS far-infrared spectra. Icarus 2009;202:620–31.
[4] Jones LH. Raman and far infrared spectrum of C_2N_2. J Mol Spectrosc 1973;45:55–64.
[5] Jolma K. The infrared spectrum of C_2N_2 in the region of the bending fundamental ν_5. J Mol Spectrosc 1982;92:33–9.
[6] Grecu JC, Winnewisser BP, Winnewisser M. High resolution Fourier transform infrared spectrum of the ν_5 fundamental band system of cyanogen, NCCN. J Mol Spectrosc 1993;159:534–50.

[7] Bermejo D, Escribano R, Santos J. The stimulated Raman spectrum of cyanogen. J Mol Spectrosc 1997;186:144–54.
[8] Maki AG, Grecu JC, Winnewisser B, Winnewisser M. High-resolution infrared spectra of $^{15}N^{12}C^{12}C^{15}N$ and $^{14}N^{13}C^{13}C^{14}N$. J Mol Spectrosc 2003;222:198–212.
[9] Maki AG. High-resolution infrared spectrum of cyanogen. J Mol Spectrosc 2011;269:166–74.
[10] Miyazawa T. Infrared absorption of cyanogen in the cesium iodide region and CN bond moment. J Chem Phys 1958;29:421–4.
[11] Kim KK, King WT. Integrated infrared intensities in cyanogen. J Chem Phys 1984;80:974–7.
[12] Botschwina P, Sebald P. Calculated spectroscopic properties for NCCN, CNCN, CNNC and HNCCN. Chem. Phys. 1990;141:311–23.
[13] Grecu JC, Winnewisser BP, Winnewisser M. Absolute rovibrational line-intensities in the ν_5 band system of cyanogen, NCCN. J Mol Spectrosc 1993;159:551–71.
[14] Jennings DE, Nixon CA, Jolly A, Bézard B, Coustenis A, Vinatier S, et al. Isotopic ratios in Titan's atmosphere from Cassini CIRS limb sounding: HC_3N in the north. Astrophys J 2008;681:L109–11.
[15] Jolly A, Fayt A, Benilan Y, Jacquemart D, Nixon CA, Jennings DE. The ν_8 bending mode of diacetylene: from laboratory spectroscopy to the detection of ^{13}C isotopologues in Titan's atmosphere. Astrophys J 2010;714:852–9.
[16] Vinatier S, Bezard B, Nixon CA. The Titan $^{14}N/^{15}N$ and $^{12}C/^{13}C$ isotopic ratios in HCN from Cassini/CIRS. Icarus 2007;191:712–21.
[17] Nixon CA, Achterberg RK, Vinatier S, Bezard B, Coustenis A, Irwin PGJ, et al. The $^{12}C/^{13}C$ isotopic ratio in Titan hydrocarbons from Cassini/CIRS infrared spectra. Icarus 2008;195:778–91.
[18] Niemann HB, Atreya SK, Bauer SJ, Carignan GR, Demick JE, Frost RL, et al. The abundances of constituents of Titan's atmosphere from the GCMS instrument on the Huygens probe. Nature 2005;438(7069): 779–84.
[19] Nixon CA, Jennings DE, Flaud J-M, Bézard B, Teanby NA, Irwin PGJ, et al. Titan's prolific propane: the Cassini CIRS perspective. Planet Space Sci 2009;57:1573–85.
[20] Tchana FK, Flaud JM, Lafferty WJ, Manceron L, Roy P. The first high-resolution analysis of the low-lying ν_9 band of propane. J Quant Spectrosc Radiat Transfer 2010;111:1277–81.
[21] Flaud JM, Tchana FK, Lafferty WJ, Nixon CA. High resolution analysis of the ν_{26} and $2\nu_9$–ν_9 bands of propane: modelling of Titan's infrared spectrum at 13.4 μm. Mol Phys 2010;108:699–704.
[22] Brown JM, Hougen JT, Huber KP, Johns JWC, Kopp I, Lefebvre-Brion H, et al. Labeling of parity doublet levels in linear molecules. J Mol Spectrosc 1975;55(1–3):500–3.
[23] Wilmes R, Winnewisser M. Preparation of mono-N-15-cyanogen and mono-C-13-cyanogen. J Labelled Compd Radiopharm 1992;31: 1037–40.
[24] Rothman LS, Gordon IE, Barbe A, Benner DC, Bernath PE, Birk M, et al. The HITRAN 2008 molecular spectroscopic database. J Quant Spectrosc Radiat Transfer 2009;110:533–72.
[25] Grecu JC, Winnewisser BP, Winnewisser M. Substitution structure of cyanogen, NCCN, from high-resolution far infrared spectra. J Mol Spectrosc 2003;218:246–55.
[26] Yamada KMT, Birss FW, Aliev MR. Effective Hamiltonian for polyatomic linear molecules. J Mol Spectrosc 1985;112:347–56.
[27] Mbosei L, Fayt A, Drean P, Cosleou J. Millimeter-wave spectra of HCCCN. J Mol Struct 2000;517:271–99.
[28] Vigouroux C, Fayt A, Guarnieri A, Huckauf A, Bürger H, Lentz D, et al. Global rovibrational analysis of HCCNC based on infrared and millimeter-wave spectra. J Mol Spectrosc 2000;202:1–18.
[29] Fayt A, Vigouroux C, Winther F. Analysis of the ν_9 band complex of dicyanoacetylene and application of a theory of relative intensities to all subbands. J Mol Spectrosc 2004;224:114–30.
[30] Amyay B, Herman M, Fayt A, Campargue A, Kassi S. Acetylene, $(12)C_2H_2$: refined analysis of CRDS spectra around 1.52 μm. J Mol Spectrosc 2011;267:80–91.
[31] Robert S, Amyay B, Fayt A, Di Lonardo G, Fusina L, Tamassia F, et al. Vibration–rotation energy pattern in acetylene: $^{13}CH^{12}CH$ up to 10120 cm^{-1}. J Phys Chem A 2009;113:13251–9.
[32] Jolly A, Benilan Y, Cané E, Fusina L, Tamassia F, Fayt A, et al. Measured integrated band intensities and simulated line-by-line spectra for C_2HD between 25 and 2.5 μm, and new global vibration rotation parameters for the bending vibrations. J Quant Spectrosc Radiat Transfer 2008;109:2846–56.
[33] Fayt A, Willaert F, Demaison J, Starck T, Mäder H, Pawelke G, et al. Fourier transform microwave spectrum of $HCCC^{15}N$ and global analysis of the high resolution infrared and rotational spectra up to 1700 cm^{-1}. Chem Phys 2008;346:115–31.
[34] Amyay B, Robert S, Herman M, Fayt A, Raghavendra B, Moudens A, et al. Vibration–rotation pattern in acetylene. II. Introduction of Coriolis coupling in the global model and analysis of emission spectra of hot acetylene around 3 μm. J Chem Phys 2009;131: 114301.
[35] Langseth A, Moller CK. The Raman spectrum and the potential function of cyanogen. Acta Chem Scand 1950;4:725–37.
[36] Maki AG. High resolution infrared spectra of cyanogen and cyanogen—$^{15}N_2$. J Chem Phys 1965;43:3193.
[37] Fish GB, Cartwright GJ, Walsh AD, Warsop PA. Rotational structure in $^1\Sigma_u^- - {}^1\Sigma_g^-$ transition of cyanogen at 2200 Å. J Mol Spectrosc 1972;41:20.
[38] Jones LH. Force field of cyanogen from vibrational spectra of isotopic species. J Mol Spectrosc 1974;49:82–90.
[39] Maki AG, Klee S. Perturbations involving ν_1 of NCCN. J Mol Spectrosc 1999;193:183–94.
[40] Albritton DL, Zare RN, Rao KN, editors. Molecular spectroscopy modern research II, vol. 1. New York: Academic Press; 1976.
[41] Botschwina P. Vibrational frequencies from anharmonic ab initio empirical potential energy functions: 5. Cyanogen—frequencies and IR intensities of stretching vibrations. Theochem J Mol Struct 1982;5:371–81.
[42] Winther F, Horneman VM, Vigouroux C, Fayt A. Analysis of the $\nu_7+\nu_9$ and $2\nu_7-\nu_9$ band complexes of dicyanoacetylene (NCCCCN). J Mol Struct 2005;742:131–46.
[43] Jacquinet-Husson N, Crepeau L, Armante R, Boutammine C, Chédin C, Scott NA, et al. The 2009 edition of the GEISA spectroscopic database. J Quant Spectrosc Radiat Transfer 2011;112:2395–445.
[44] Benilan Y, Jolly A, Raulin F, Guillemin J-C. IR band intensities of DC_3N and $HC_3^{15}N$: implication for observations of Titan's atmosphere. Planet Space Sci 2006;54:635–40.
[45] Weber M, Blass WE, Halsey G, Hillman J. Resonance perturbation of IR intensities in C_2H_2 near 13.7 μm. J Mol Spectrosc 1994;165: 107–23.
[46] Jacquemart D, Claveau C, Mandin J-Y, Dana V. Line intensities of hot bands in the 13.6 μm spectral region of acetylene C_2H_2. J Quant Spectrosc Radiat Transfer 2001;69:81–101.